Model Predictive Anti-Jerk Control of an Electrified Drivetrain with Backlash

Submitted by

Jomar-Christian Noceda

Mechanical Engineering

To

The Honors College

Oakland University

In partial fulfillment of the

requirement to graduate from

The Honors College

Mentor: Dr. Yongsoon Yoon, Assistant Professor

Department of Mechanical Engineering

Oakland University

December 2, 2022

Abstract

This thesis addresses an optimal anti-jerk control law of an electrified drivetrain based on a model predictive control scheme. Due to a flexible driveshaft and gear clearance in the electrified drivetrain, when the vehicle traction torque changes drastically, it undergoes torsional vibration made more severe by the lack of external damping elements compared to the drivetrain in a gas-powered vehicle. This leads to unpleasant longitudinal vibration of a vehicle, so called jerk. This longitudinal vibration adversely affects driving comfort of an occupant which is undesirable with the growing trend toward automotive electrification. Although excessive damping can mitigate the torsional vibration of the drivetrain and improve driving comfort, it deteriorates vehicle responsiveness to the driver's torque demand. Therefore, an optimal control law compromising these two conflicts is important. Toward this end, this thesis aims to develop the model predictive anti-jerk control law to find a trade-off between driving comfort and vehicle responsiveness.

Table of Contents

I. Introduction

Electrification of the Automotive Industry

Electric vehicles (EVs) are being pushed to the forefront of the automotive industry. One of the major factors is the increasing alarm of global warming and air pollution. Global warming is the result of greenhouse gases such as carbon dioxide and methane in the atmosphere trapping the energy of the Sun's reflected infrared radiation from the ground, causing a greenhouse effect [1]. This leads to increased global temperatures, natural disasters, and ecological crises. In 2019, the United States Environmental Protection Agency (EPA) recorded that the leading contributor of greenhouse gas emissions that came from the burning of fossil fuels was by cars, trucks, and other forms of transportation which accounted for 29% of emissions [2]. Despite the lockdown mandates of the pandemic in 2020, the transportation sector was still the leading emitter of greenhouse gases in the U.S., accounting for 27% of emissions [3].

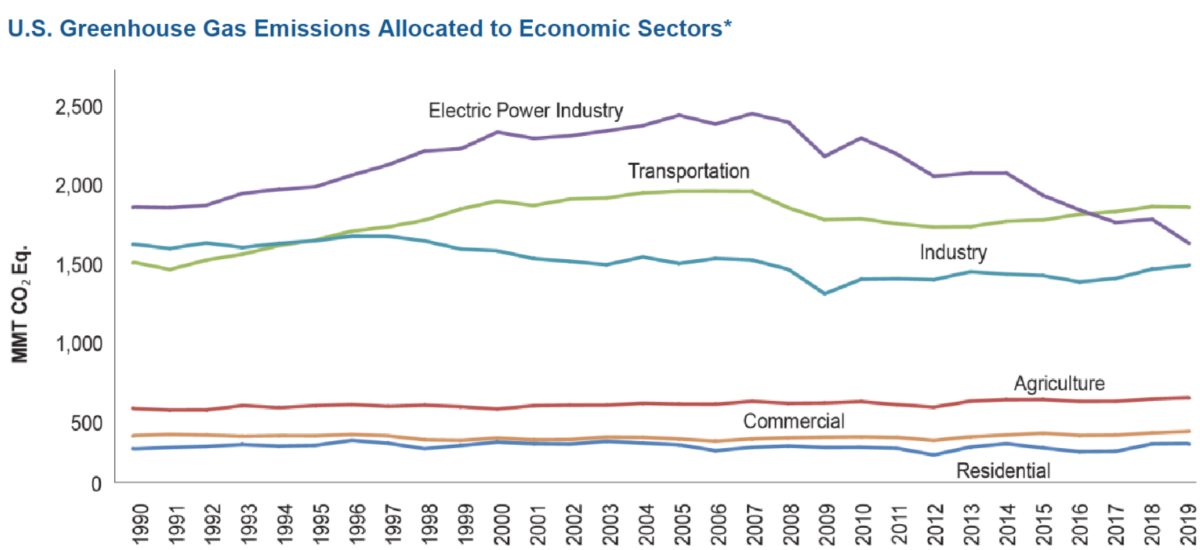

Figure 1: EPA report on the total emissions by sector from 1990 to 2019 [2]

Consequently, policy makers around the world are pushing for the electrification of the automotive industry to help reduce greenhouse gas emissions. The European Parliament and Canada are in support of plans to prohibit the sale of new gas and diesel cars by 2035, and California is expected to follow suit with a similar plan [4]. News of these policies are motivating car manufacturers to prioritize electric vehicle development and for some to commit to all-electric vehicle lineups in the near future. By 2030, both Toyota and General Motors plan to offer around 30 fully-electric vehicle models while Ford and BMW plan to have 50% of sales be fully-electric models [5]. Even with the initiatives taken by governments and car manufacturers, certain conditions must be met for EVs to be a convincing alternative to internal combustion engine (ICE) vehicles. These conditions include lower vehicle prices, longer travel ranges, quicker charging times, and an extensive charging infrastructure. As these conditions continue to be met, drivability will become an even more important point of comparison between ICE and electric vehicles.

Lack of Damping in an EV Driveline

In the 1970s, drivability criteria consisted of fuel consumption and emissions whereas now it deals with characteristics such as a vehicle’s operating responsiveness, smoothness, and comfort [6]. EVs use electric motors to drive the wheels. The instantaneous peak torque that electric motors deliver from standstill is an advantage in responsiveness over internal combustion engines, however, this can be detrimental to the comfort of the vehicle’s occupants. EVs have fewer mechanical driveline components compared to ICE vehicles. An important component present in ICE vehicles that is lacking in EVs is a coupling like a clutch or torque converter that provides a soft connection between the engine and transmission [1]. The rigid connection of the motor to the rest of the driveline in an EV results in low damping [6]. This means that with a rapid change in requested torque with the pressing the accelerator pedal, the driver experiences unpleasant longitudinal vibrations, referred to as jerk, that are more sustained [7].

Vehicle Clunk and Shuffle

The vehicle jerk is a result of torsional vibrations being transferred through the driveshaft and to the wheels. A rapid change in the requested torque caused by pressing or releasing the accelerator pedal is referred to as a vehicle tip-in or tip-out event, respectively. The torsional vibrations, and consequently the vehicle jerk, that follow shortly after can be attributed to two main factors: a flexible driveshaft and gear clearance in the drivetrain. The driveshaft within a vehicle is made of material that is subject to twisting. When a torque is applied at one end of the shaft, the elasticity in the driveshaft causes a difference in angle with the other end which excites a low-frequency vibrational mode known as shuffle [8]. The frequency of this shuffle is between 1-15 Hz and overlaps with the resonance frequency of human organs, leading to discomfort [9]. The shuffling phenomenon can be seen in Fig. 2 below after a tip-in event occurs at a time of 25 seconds.

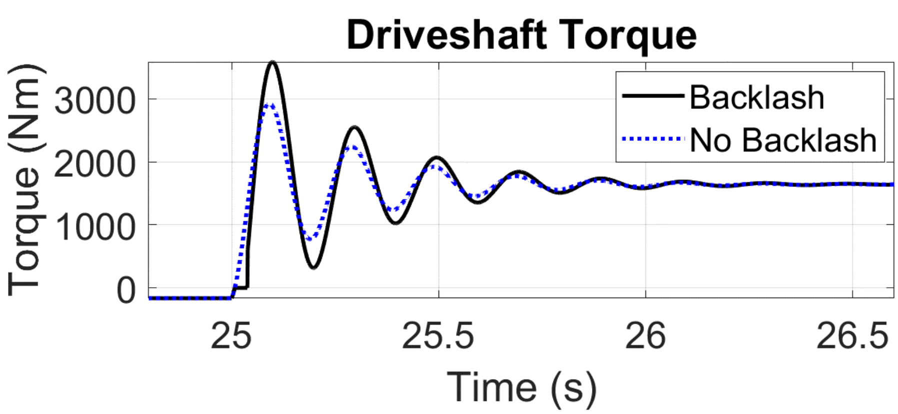

Figure 2: Torsional oscillations after a tip-in event

The gearbox and half shafts that transfer torque from the motor to the wheels are composed of gears. The teeth between meshed gears have a small amount of clearance which is referred to as backlash and is displayed in Fig. 3. Backlash is inevitable with any set of gears since manufacturing parts with tight tolerances is expensive and parts wear out over time eventually. Backlash is even desired in some cases for lubrication purposes [10].

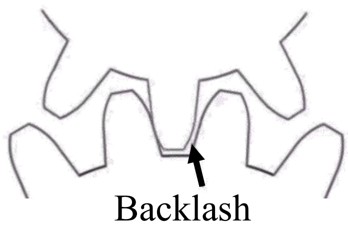

Figure 3: A set of meshed gears with clearance

This backlash must be traversed first in order for torque to be transferred between gears. During the traversal of the backlash, the driven gear moves independently from the driving gear causing it to increase in speed relative to the driving gear [11]. After the backlash is traversed, there is a hard and noisy impact due to the speed difference once the gears come into contact again, which is referred to as clunk [12]. As evident in Fig. 2, the inclusion of backlash in the system leads to an increase in amplitude of driveline oscillation which further deteriorates drivability [13].

Proposed Control Strategy

The objective of the drivetrain anti-jerk controller is to traverse backlash quickly and reach the demand torque from the driver as soon as possible while avoiding vibrations. When it comes to controlling vehicle jerk, a control strategy growing in popularity involves model predictive control (MPC) which finds a set of optimal control inputs over a finite look-ahead horizon [14,15]. A majority of existing MPC-based works in control literature are based on an implicit MPC, which solves a constrained optimization problem in real time [6, 16, 17]. In this thesis, an explicit MPC is proposed to control unpleasant vibrations. An explicit MPC finds an optimal solution offline and control parameters are mapped as a function of model parameters or operating conditions and stored in a control unit. Its computational cost is much lower than that of the implicit MPC which makes it more feasible to implement into an actual vehicle controller. However, because of the lack of flexibility to change the control parameters once they are stored in a control unit, robustness to model uncertainties should be taken into consideration. By making the control law robust, it will ensure that the vehicle performance and comfort is sufficient regardless of external disturbances or uncertainties in vehicle parameters over time. Additionally, a feedforward controller will be paired with the explicit MPC to further reduce vibrations. The feedforward controller uses the torque demand from the driver and employs dynamic rate limiting to ensure there is not a significant loss of responsiveness.

Structure of Thesis

This paper is divided into the following chapters: Dynamic Modeling, Simulation Model Development, Open-Loop Analysis, Feedforward Control, Feedback Control, Conclusion, and Future Work. In the Dynamic Modeling chapter, the dynamics of the driveline model will be derived using a physics-based method. Then, the Simulation Model Development chapter will go through the programming of the driveline dynamics into the Simulink software. The Open-Loop Analysis chapter will review simulations from the Simulink model without the proposed control method. The Feedforward Control chapter will go over the method of dynamic rate limiting and will include simulations with it implemented into the Simulink model and its improvements over the open-loop system. The Feedback Control chapter will derive, compare, and simulate the proposed explicit MPC with a baseline LQR controller. The Conclusions chapter will summarize the main contributions of this thesis. The Future Work chapter will discuss topics that will be further researched into.

II. Dynamic Modeling

Two-Inertia Model

The main components of the electrified drivetrain include the electric motor, gearbox, driveshaft, and wheel. The motor generates torque which undergoes a gear reduction via a gearbox. The torque is then transmitted to a flexible driveshaft. Before the torque can finally be transferred to the wheels, the backlash throughout the driveline must be traversed first. The drivetrain dynamics can be represented by a two-inertia model as shown below in Fig. 4.

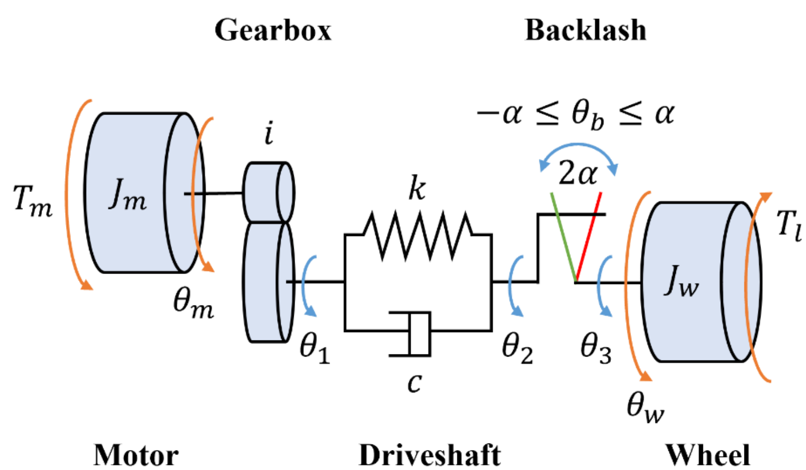

Figure 4: Electrified driveline represented by a two-inertia model

The rotating inertia denoted with J_m is comprised of the lumped inertias of the motor and gearbox. The rotating inertia J_w denotes the load inertia which is made up of the lumped inertias of the wheel and vehicle. The driveshaft is the most flexible component and can be represented by a spring and damper element with stiffness coefficient *k* and damping coefficient *c*. Between the driveshaft and the wheel is the backlash element that consists of the lumped backlash throughout the driveline. The backlash position θ_b can vary from an angle of -α to α which means the total size of the backlash is an angle of 2α. As proven in [9], it is acceptable to lump inertia elements such as in the two-inertia model above since it is simpler to use in control applications and it replicates the shuffling behavior of a full-order model with 24 inertias with less than 5% error. It was also proven in [9] that lumping all backlash elements at the end of the driveshaft resulted in the same backlash traversal times as a system with multiple backlash elements distributed throughout the driveline. Therefore, the two-inertia model with a single backlash element was chosen for control design.

In the model above, it is helpful to define certain angles. As termed by [18], the displacement angle θ_d is the difference between the angle of the motor after the gear reduction and the angle of the wheel which can be expressed as

$$\theta_d = \theta_1 - \theta_3 \tag{1}$$

$$\theta_d = \frac{1}{i}\theta_m - \theta_w \tag{2}$$

The shaft twist θ_s can be defined by the difference in angle between the input and output ends of the driveshaft before the backlash element.

$$\theta_s = \theta_1 - \theta_2 \tag{3}$$

The backlash position θ_b is defined by the difference in angle between the output end of the driveshaft and the angle of the wheel.

$$\theta_b = \theta_2 - \theta_3 \tag{4}$$

The shaft twist can be expressed using the displacement angle and backlash angle.

$$\theta_s = \theta_d - \theta_b \tag{5}$$

Physics-Based Derivation

Using Newton's second law for rotational motion, the dynamics of the motor and load inertia can be derived. It is important to note that during the traversal of backlash, or when $-\alpha \leq \theta_b \leq \alpha$, the motor is effectively disconnected from the wheels meaning the driveshaft does not transmit any torque. Therefore, the system can be divided into three different modes. If θ_b is at -α, the system is in negative contact mode. If θ_b is at α, the system is in positive contact mode. The system is in backlash mode when the backlash position θ_b is between -α and α.

Positive and Negative Contact Mode Dynamics

$$J_m \dot{\omega}_m = T_m - \frac{T_s}{i} \tag{6}$$

$$J_w \dot{\omega}_w = T_s - T_l \tag{7}$$

$$\dot{\theta}_b = \begin{cases} max\left(0, \dot{\theta}_d + \frac{k}{c}(\theta_d - \theta_b)\right), \text{if } \theta_b = -\alpha \\ min\left(0, \dot{\theta}_d + \frac{k}{c}(\theta_d - \theta_b)\right), \text{if } \theta_b = \alpha \end{cases} \tag{8}$$

Backlash Mode Dynamics

$$J_m \dot{\omega}_m = T_m \tag{9}$$

$$J_w \dot{\omega}_w = -T_l \tag{10}$$

$$\dot{\theta}_b = \dot{\theta}_d + \frac{k}{c}(\theta_d - \theta_b) \tag{11}$$

The backlash dynamics in Eqs. (8) and (11) are from the physical backlash model derived in [18] which is favored for its physically accurate behavior for a shaft with both stiffness and damping. Further analyzing Eq. (8), if the system is in negative contact mode with $\theta_b = -\alpha$, then $\dot{\theta}_b$ cannot decrease further since θ_b is already at its lower limit, so $\dot{\theta}_b$ remains at zero. The general condition for the backlash gap to open is a change in the sign of the torque with respect to the contact mode. If the system is in negative contact mode, a positive torque request will cause the system to enter backlash mode until the upper limit is reached. This is because a positive torque will cause the motor to increase in speed relative to the wheel, which will lead to $\dot{\theta}_d$ eventually surpassing the $\frac{k}{c}(\theta_d - \theta_b)$ term in Eq. (8). As a result of these dynamics, a negative shaft torque can only be transmitted in negative contact mode and vice versa. A summary of the conditions needed for the system to change modes is shown in Fig. 5.

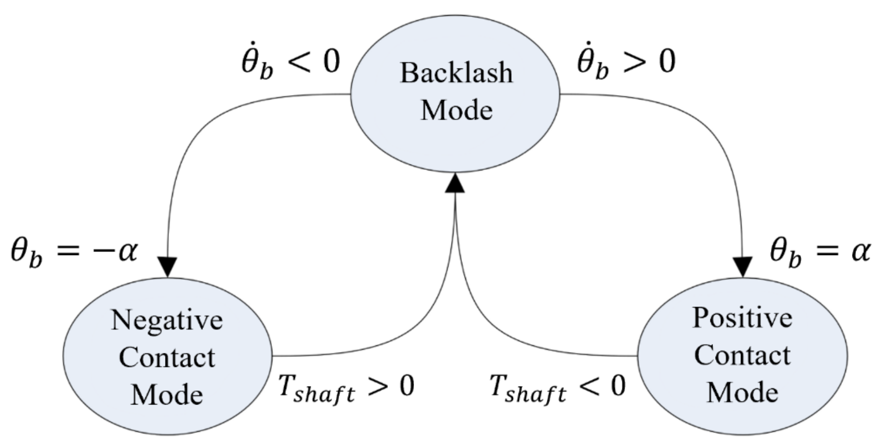

Figure 5: Conditions for model mode changes

The dynamics of the system can be expanded by considering that the driveshaft torque T_s is equivalent to the torques of the torsional spring and damper that represent the driveshaft [19].

$$T_s = k(\theta_s) + c(\dot{\theta}_s) \tag{12}$$

The shaft twist can be expanded using Eqs. (5) and (2). Additionally, driveshaft torque is only transmitted in contact mode where the backlash position is not changing.

$$T_s = k(\theta_d - \theta_b) + c(\dot{\theta}_d - \dot{\theta}_b) \tag{13}$$

$$T_s = k\left(\left(\frac{1}{i}\theta_m - \theta_w\right) - \theta_b\right) + c\left(\frac{1}{i}\omega_m - \omega_w\right) \tag{14}$$

Using Eq. (14), the contact-mode and backlash-mode dynamics can be expanded with variables for the motor and wheel.

Positive and Negative Contact Mode Dynamics

$$J_m\dot{\omega}_m = T_m - \frac{k}{i^2}\theta_m - \frac{c}{i^2}\omega_m + \frac{k}{i}\theta_w + \frac{c}{i}\omega_w + \frac{k}{i}\theta_b \tag{15}$$

$$J_w\dot{\omega}_w = \frac{k}{i}\theta_m + \frac{c}{i}\omega_m - k\theta_w - c\omega_w - k\theta_b - T_l \tag{16}$$

$$\dot{\theta}_b = \begin{cases} max\left(0, \frac{k}{ci}\theta_m + \frac{1}{i}\omega_m - \frac{k}{c}\theta_w - \omega_w - \frac{k}{c}\theta_b\right), \text{if } \theta_b = -\alpha \\ min\left(0, \frac{k}{ci}\theta_m + \frac{1}{i}\omega_m - \frac{k}{c}\theta_w - \omega_w - \frac{k}{c}\theta_b\right), \text{if } \theta_b = \alpha \end{cases} \tag{17}$$

Backlash Mode Dynamics

$$J_m\dot{\omega}_m = T_m \tag{18}$$

$$J_w\dot{\omega}_w = -T_l \tag{19}$$

$$\dot{\theta}_b = \frac{k}{ci}\theta_m + \frac{1}{i}\omega_m - \frac{k}{c}\theta_w - \omega_w - \frac{k}{c}\theta_b \quad (20)$$

The variables and their descriptions are summarized in Table 1.

Table 1. Model Variables

Symbol	Descriptions	Units
J_m	Moment of inertia of motor and gearbox	[kg·m²]
J_w	Moment of inertia of wheel and vehicle	[kg·m²]
θ_m	Angular position of motor	[rad]
θ_w	Angular position of wheel	[rad]
θ_b	Angular position of backlash	[rad]
ω_m	Angular speed of motor	[rad/s]
ω_w	Angular speed of wheel	[rad/s]
i	Fixed gear ratio	[-]
T_m	Generated motor torque	[N·m]
T_l	Load torque	[N·m]
k	Spring coefficient of driveshaft	[N·m/rad]
c	Damping coefficient of driveshaft	[N·m·s/rad]

III. Simulation Model Development

Simulation models are crucial in control design as they are an inexpensive way to test the performance of a controller without implementing it into a full-sized test vehicle or test bench. The model dynamics derived in the last section were programmed into a Simulink model to run simulations of the driveline. The Simulink model will be important in analyzing the dynamics of the system both without control and with the proposed controller. The programmed electrified driveline with backlash is shown in Fig. 6 below. Five different sections are marked off in red and will be explained further.

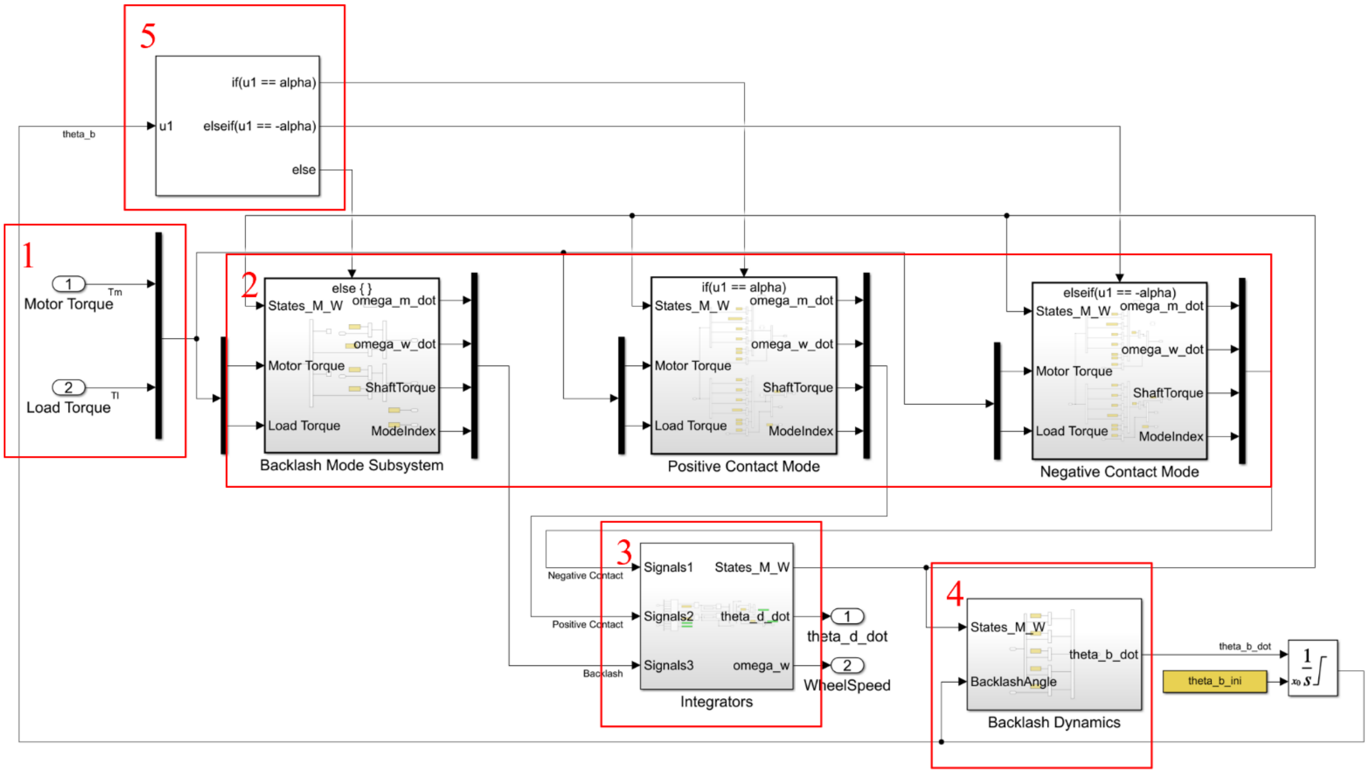

Figure 6: Electrified drivetrain model programmed in Simulink

The first section of the Simulink model in Fig. 6 are the inputs to the system which are the motor torque and load torque. The motor torque input is interpreted as the torque demand by the driver when the acceleration pedal is pressed or released. The load torque is generally unknown as it can be impacted by factors such as bumps in the road surface or changes in wind speed. For the purposes of the simulation, driving resistances which are functions of vehicle speed such as rolling resistance, grade resistance, and aerodynamic resistances were considered.

The second section of the model consists of subsystem blocks for the three different modes that the system can be in. These subsystems are programmed with Eqs. (15) and (16) for contact mode, and with Eqs. (18) and (19) for backlash mode. These equations are easy to implement since they utilize the motor and wheel angular positions and speeds. The equations for backlash dynamics are programmed in a different section. The inputs of all three subsystems consist of the motor torque, load torque, and the states of the motor and wheel that are looped back from the next section. Each subsystem calculates the motor and wheel angular acceleration as well as the shaft torque for their respective system mode. The angular accelerations are then input into the third section which integrates these signals to obtain the angular speeds and positions of the motor and wheel.

The fourth section of the model calculates the rate at which the backlash position changes $\dot{\theta}_b$ based on Eq. (20). The backlash rate that is output by the subsystem is then integrated to obtain the backlash position. The backlash position is then used by the If-Else Block to determine which driveline mode is active based on the criteria described in the last chapter. Only the driveline mode subsystem that is active will have its signals pass through the integrator blocks in the third section.

In the next section, the dynamics of the model will be validated by running simulations of the Simulink program without any active-damping controller.

IV. Open-Loop Analysis

Vehicle Parameters

To run the programmed model, the vehicle parameters must be identified first. The parameters given in Table II were adopted from [10] and are for a utility van that underwent an electric conversion. In [10], the parameters were determined using grey-box modeling which utilizes logged testing data and a mathematical model of the system to calculate unknown values.

Table 2. Vehicle Parameters

Symbol	Descriptions	Value	Units
J_m	Moment of inertia of motor and gearbox	0.1462	[kg·m²]
J_w	Moment of inertia of wheel and vehicle	203.48	[kg·m²]
2α	Total backlash size	2×0.05	[rad]
i	Fixed gear ratio	8.658	[-]
k	Spring coefficient of driveshaft	10556	[N·m/rad]
c	Damping coefficient of driveshaft	90	[N·m·s/rad]

Open-Loop Numerical Simulation

The first event of the simulation is a tip-in maneuver where the vehicle is initialized with a positive torque request at a time of 10 seconds as seen in Fig. 7a below. The model is initially in positive contact mode as evident with the backlash position θ_b being at +α, so positive contact mode is retained when a positive torque is requested. Since the backlash gap is not opened, the oscillations in the driveshaft torque can be mainly attributed to the driveshaft flexibility. As can be seen in Fig. 7b, these torsional oscillations lead to shuffling in the longitudinal vehicle acceleration with a frequency of around 4.3 Hz which is perceived as an uncomfortable jerking motion to the driver and passengers. This shuffling takes around 1.2 seconds to converge. The motor speed is also subject to oscillations since the other end of the flexible driveshaft is connected to the vehicle and wheel inertia which is substantially larger than the motor and gearbox inertia. The twisting of the driveshaft causes the input end connected to the motor to oscillate in speed until the rate at which the driveshaft is twisting, the torsion rate, converges to zero.

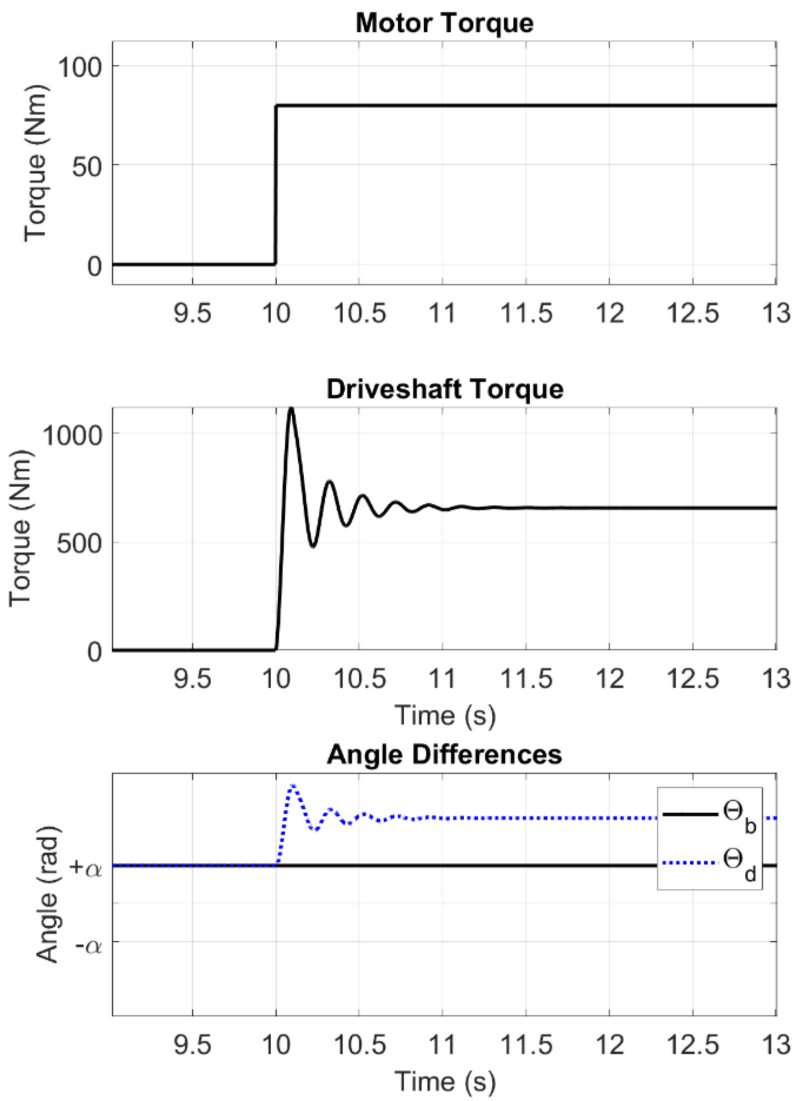

Figure 7a: Open-loop tip-in maneuver with no backlash traversal

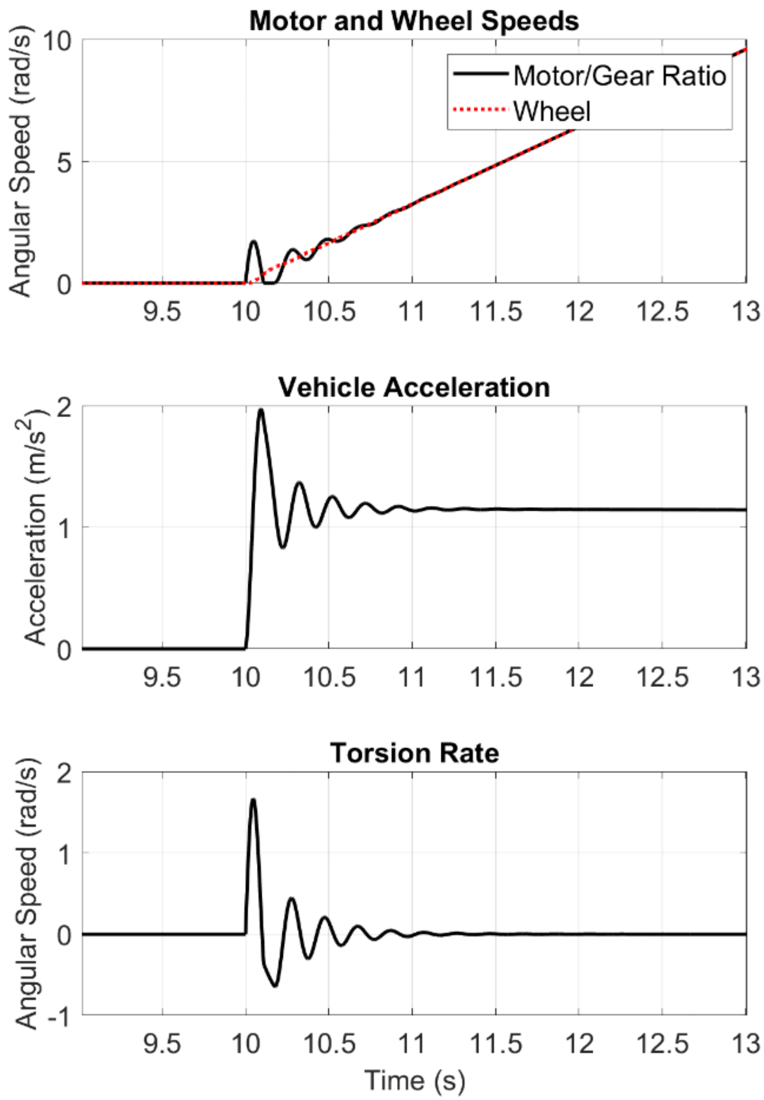

Figure 7b: Open-loop tip-in maneuver with no backlash traversal

After gaining some speed, the acceleration pedal is released at a time of 15 seconds, and a positive torque is no longer requested. Due to regenerative braking, the motor is being run as a generator which leads to negative motor torque during coasting conditions as seen in Fig. 8a below. Because there is a change in sign of the torque, the backlash gap opens as seen with θ_b moving from +α to -α.

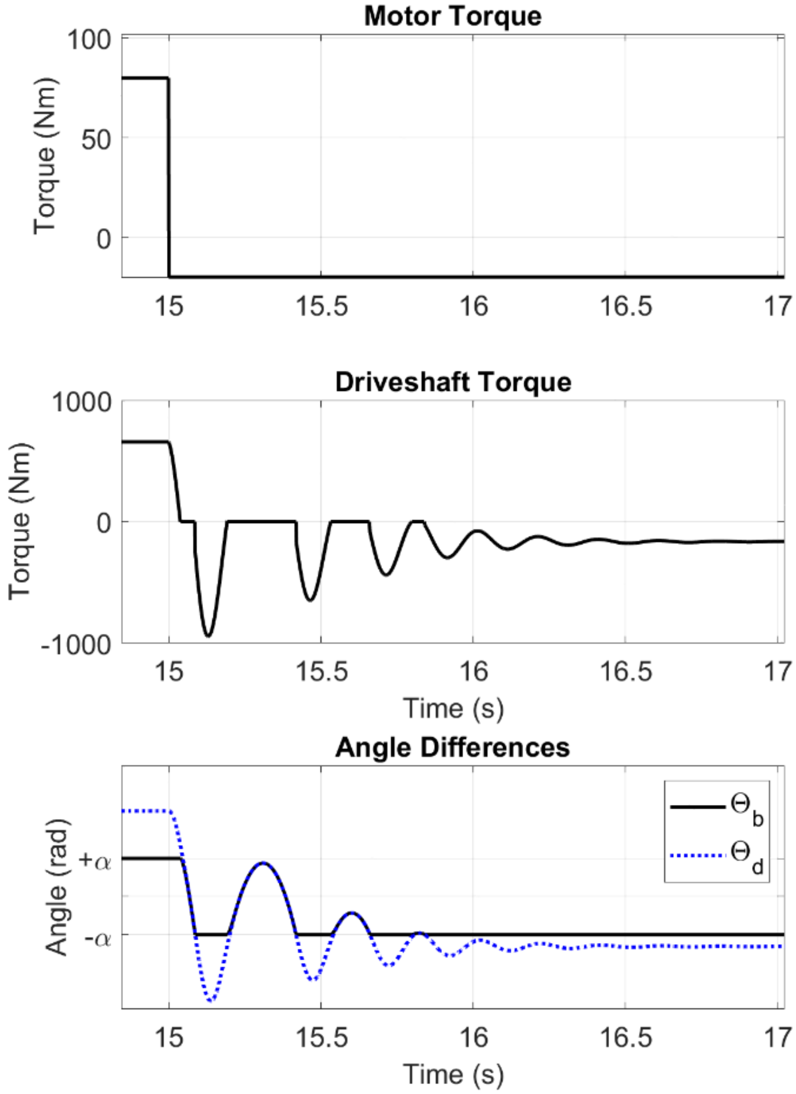

Figure 8a: Open-loop tip-out maneuver with backlash traversal

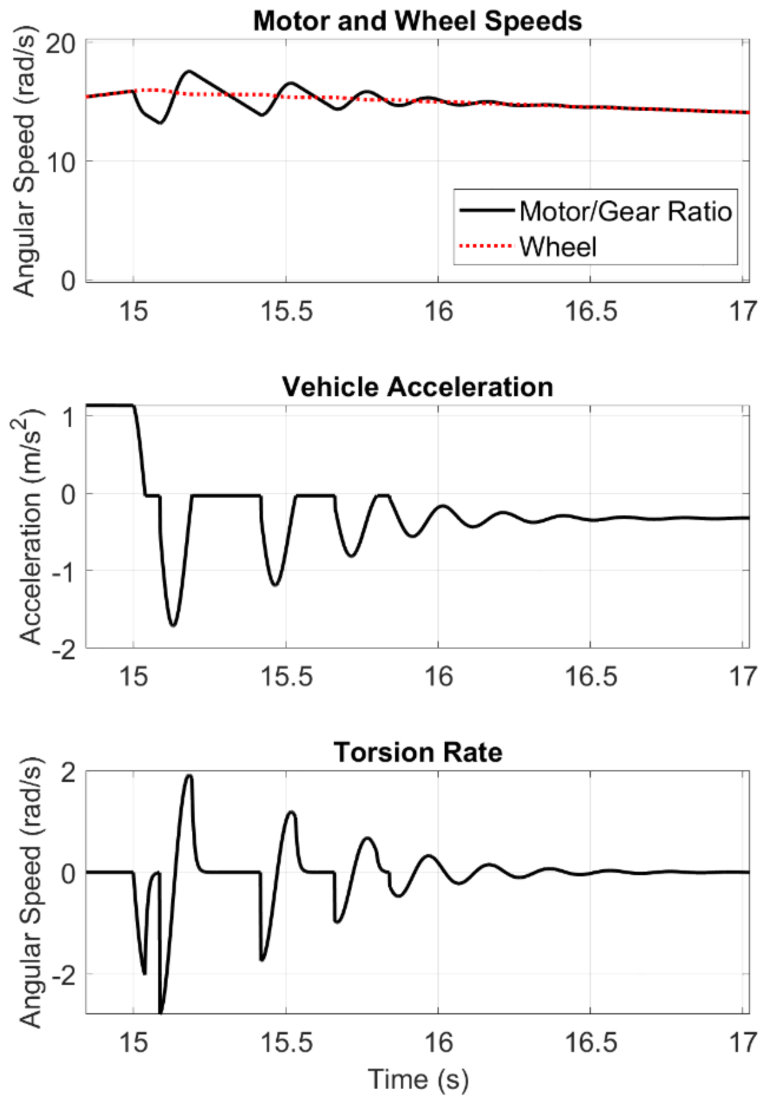

Figure 8b: Open-loop tip-out maneuver with backlash traversal

The motor and wheel are effectively disconnected when the system enters backlash mode which means torque cannot be transmitted as seen with the driveshaft torque zeroing out. It can also be seen in Fig. 8a that the shaft twist, or the difference between the displacement angle θ_d and the backlash position θ_b, is zero during backlash traversal. Since the driveshaft stiffness is much larger than the driveshaft damping, it should not be twisting in backlash mode [12]. After the negative contact side is reached at about 15.09 seconds, the driveshaft is able to transmit negative torque. However, the oscillating nature of the driveshaft twist actually causes the backlash gap to open several times. This same phenomenon is observed in [20]. As a result, the vehicle's acceleration is interrupted intermittently as seen in Fig. 8b. This leads to the frequency of shuffling to be lower and thus, more perceivable to the occupants of the vehicle.

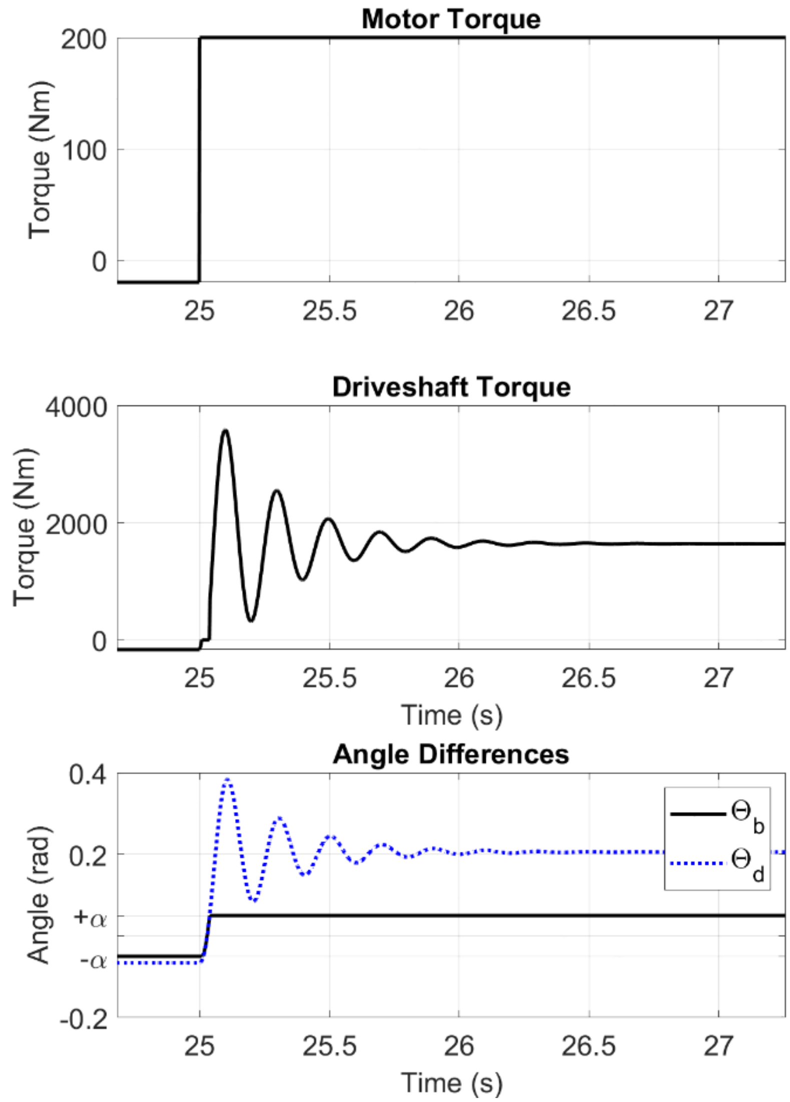

Figure 9a: Open-loop tip-in maneuver with backlash traversal

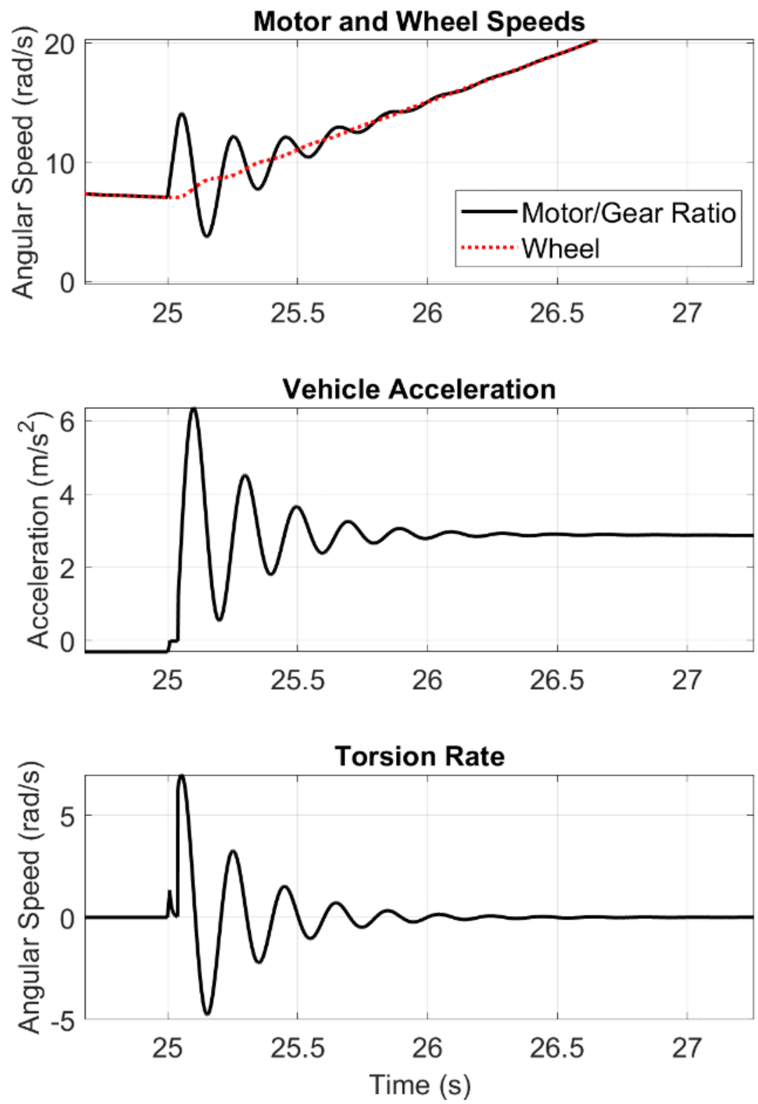

Figure 9b: Open-loop tip-in maneuver with backlash traversal

Next, a more drastic tip-in maneuver is commanded at a time of 25 seconds with 200 Nm of torque being requested as shown in Fig. 9a above. The motor rapidly increases in speed when traversing the backlash from 25-25.04 seconds as shown in Fig. 9b. When positive contact is reached the motor speed oscillates before increasing steadily with the wheel speed. Notably, the magnitude of the shaft twist, as shown by the difference between θ_d and θ_b, is large enough that the system does not enter backlash mode for a second time. The magnitude of all oscillations is increased due to the higher torque demand, especially the torsion rate. Therefore, an effective control strategy is needed to dampen vibrations.

V. Feedforward Control

The presence of backlash makes the driveline model highly nonlinear and therefore complex to control. Since the motor can be decoupled from the wheel, it is difficult to estimate measurements such as the backlash position, especially since backlash traversals can be as quick as 0.04 seconds which do not allow sufficient convergence time for an estimator or observer. Coupling a feedforward controller along with a feedback controller allows for improved stability compared with just a feedback controller alone [21, 22]. This is because a feedforward controller can take corrective action before the system's response becomes problematic as is the case with excessive torsional vibrations in the driveline during a tip-in or tip-out maneuver.

Feedforward Control Design

Torque profiling is a feedforward method that can reduce the bad effects of backlash on the drivetrain since it lessens the impact velocity of the gear after traversing backlash [23]. This can reduce the severity of vibrations, but it is important to ensure that the vehicle's responsiveness is not severely deteriorated. The proposed torque profiling method utilizes the dynamic rate limiter block in Simulink as seen in Fig. 10 which can adjust the maximum rate of change of the motor torque.

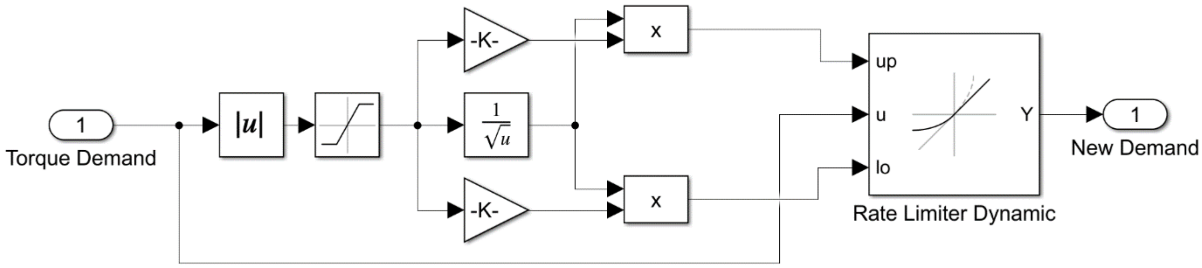

Figure 10: Feedforward subsystem block

The positive and negative rate limits are programmed with the following expression:

$$|\text{Rate Limit}| = K_{ff}\frac{|d(t)|}{\sqrt{|d(t)|}} \tag{21}$$

The torque request by the driver $d(t)$ is input into the feedforward controller and is multiplied with an empirically determined gain K_{ff} to calculate the rate limit. Dividing $d(t)$ with its square root ensures that responsiveness is maintained when a smaller torque is requested by the driver. Additionally, a lower limit is applied to $d(t)$ to ensure the denominator is non-zero. Numerical simulations with only the feedforward controller implemented are compared to a system without any controller.

Feedforward Numerical Simulation

At a time of 10 seconds, a torque of 80 Nm is requested as shown in Fig. 11a. The system is in positive contact mode before and after the torque request. With no controller, the full torque request is commanded instantly while with the feedforward controller, the torque request is reached 0.15 seconds later. The minimal loss in performance is evident in the vehicle speed shown in Fig. 11b where the system with feedforward control active starts speeding up at the same rate shortly after the system without any control. Oscillations in the driveshaft torque and the motor speed are also dampened with feedforward control. While convergence time is similar for both no controller and feedforward control, the initial peak of the driveshaft torque is reduced by 28% which also reduces the intensity of vehicle jerk.

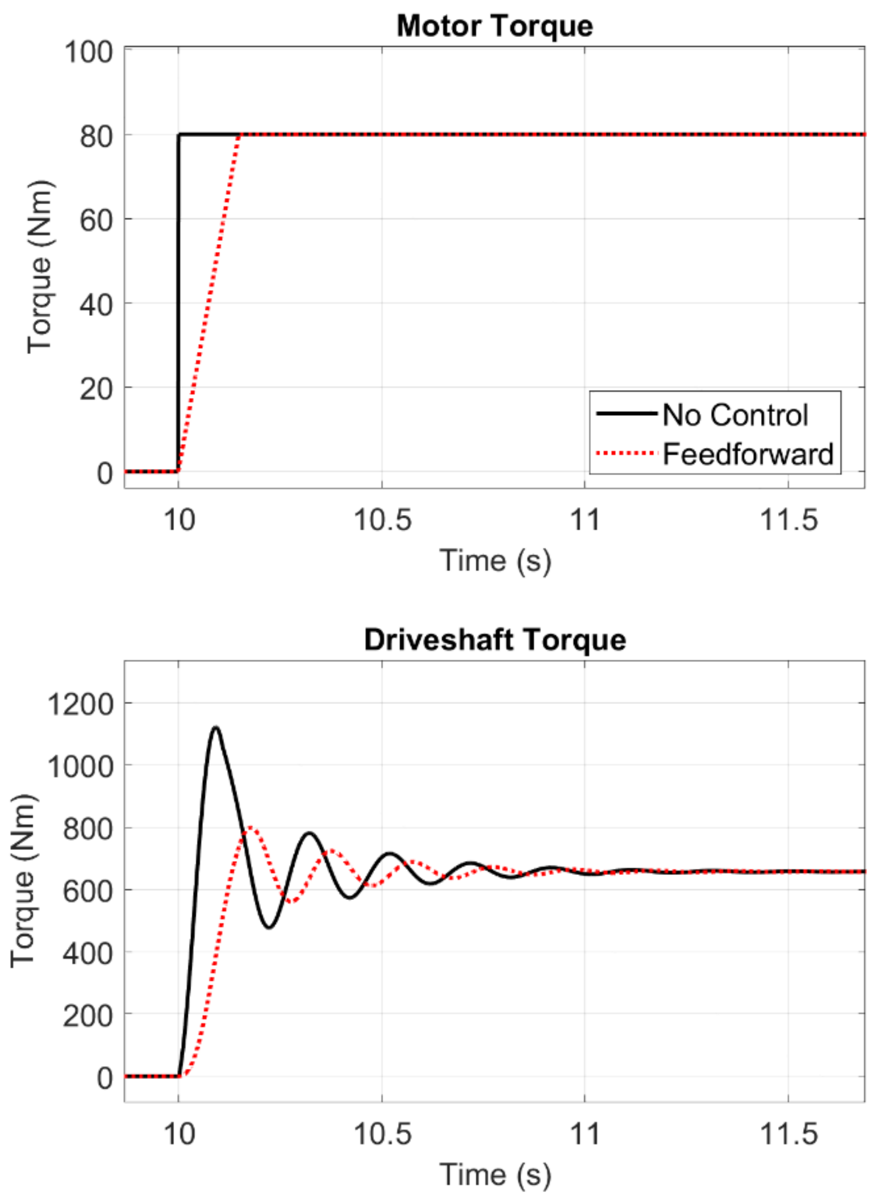

Figure 11a: Feedforward vs. open-loop tip-in maneuver with no backlash traversal

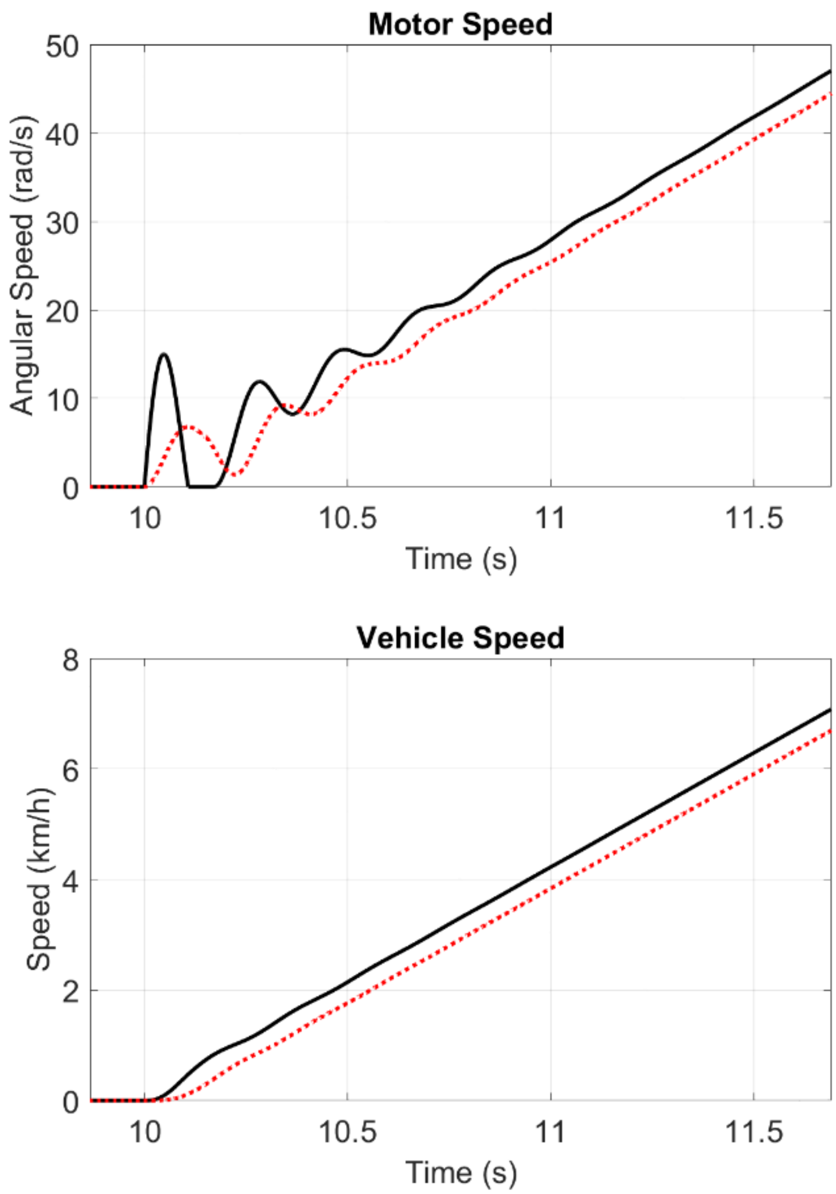

Figure 11b: Feedforward vs. open-loop tip-in maneuver with no backlash traversal

At a time of 15 seconds, a tip-out event occurs. Due to the change in sign of the motor torque request, the backlash gap must be traversed before reaching negative contact mode. As shown in Fig 12a below, the time it takes for the feedforward control to reach the demanded torque is around 0.18 seconds. The system with feedforward control causes the motor speed to decrease slower which leads to a reduction in impact velocity when the other side of the backlash is reached. As a result, the overshoot in driveshaft torque is reduced and the system enters backlash mode one less time than the system with no control. This is beneficial because reducing the number of times the gears impact after traversing backlash leads to longer part life.

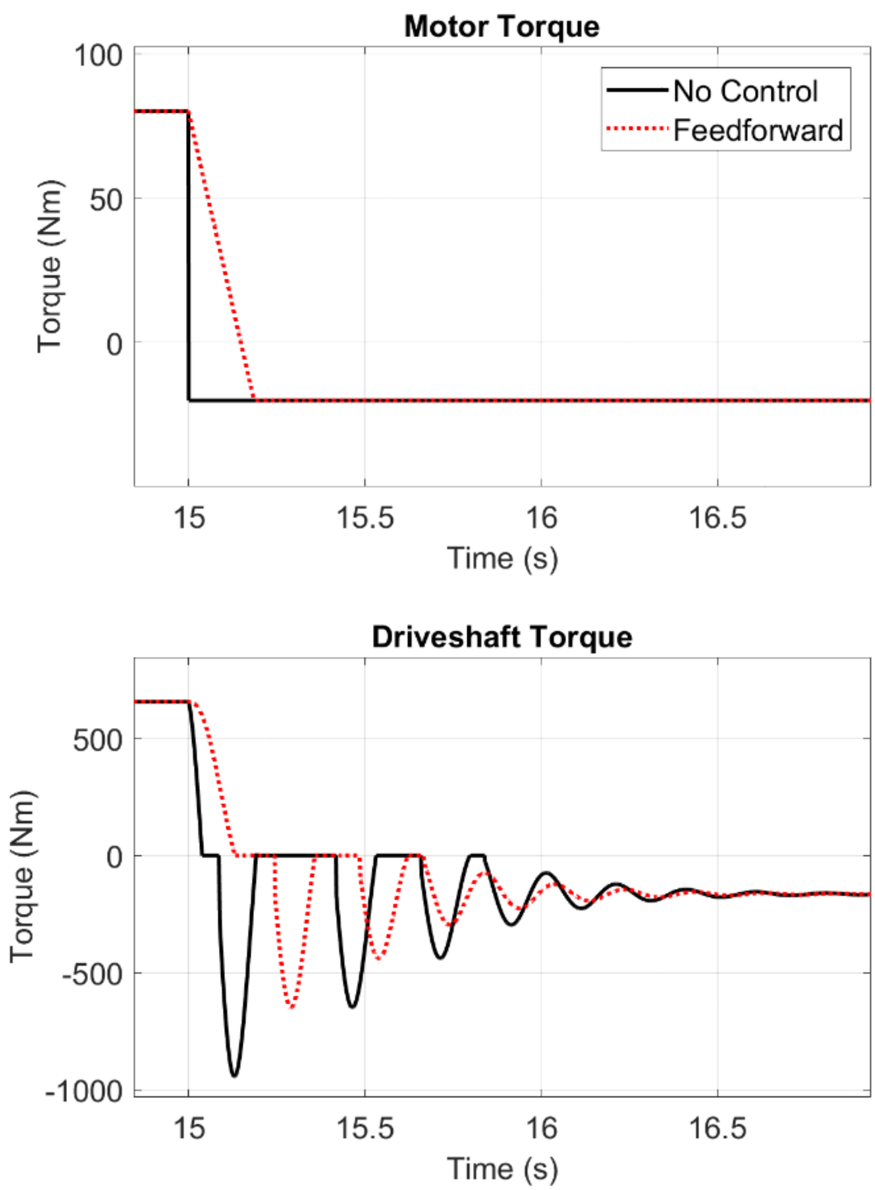

Figure 12a: Feedforward vs. open-loop tip-out maneuver with backlash traversal

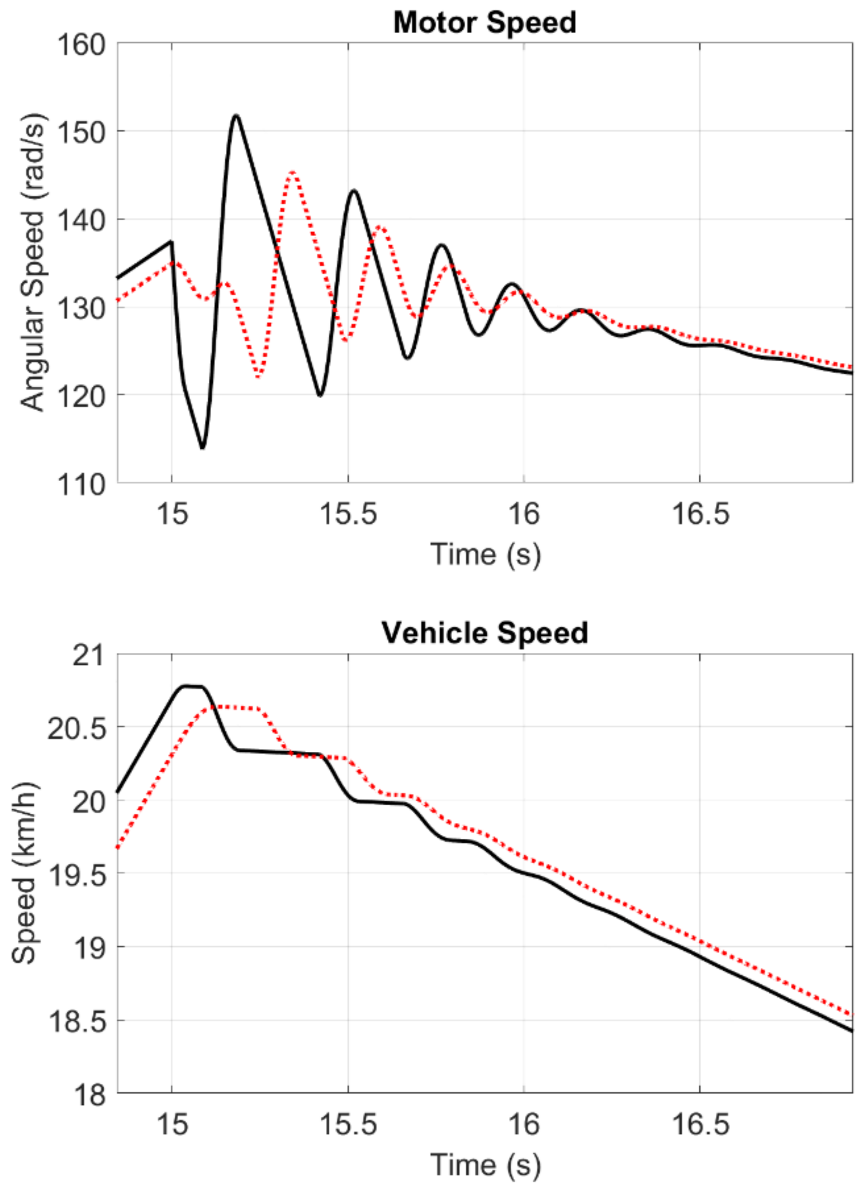

Figure 12b: Feedforward vs. open-loop tip-out maneuver with backlash traversal

In Figure 13a, a more drastic tip-in is requested. For the system with feedforward control, the demand torque of 200 Nm is reached after 0.26 seconds. The backlash traversal only takes .034 seconds longer and yet the speed with which the other side of the backlash is impacted with is much less than the system with no control as evident by the reduced amplitude in oscillations of both the driveshaft torque in Fig. 13a and motor speed in Fig. 13b. Notably, the initial peak of the driveshaft torque is reduced by 49% with the implemented feedforward control.

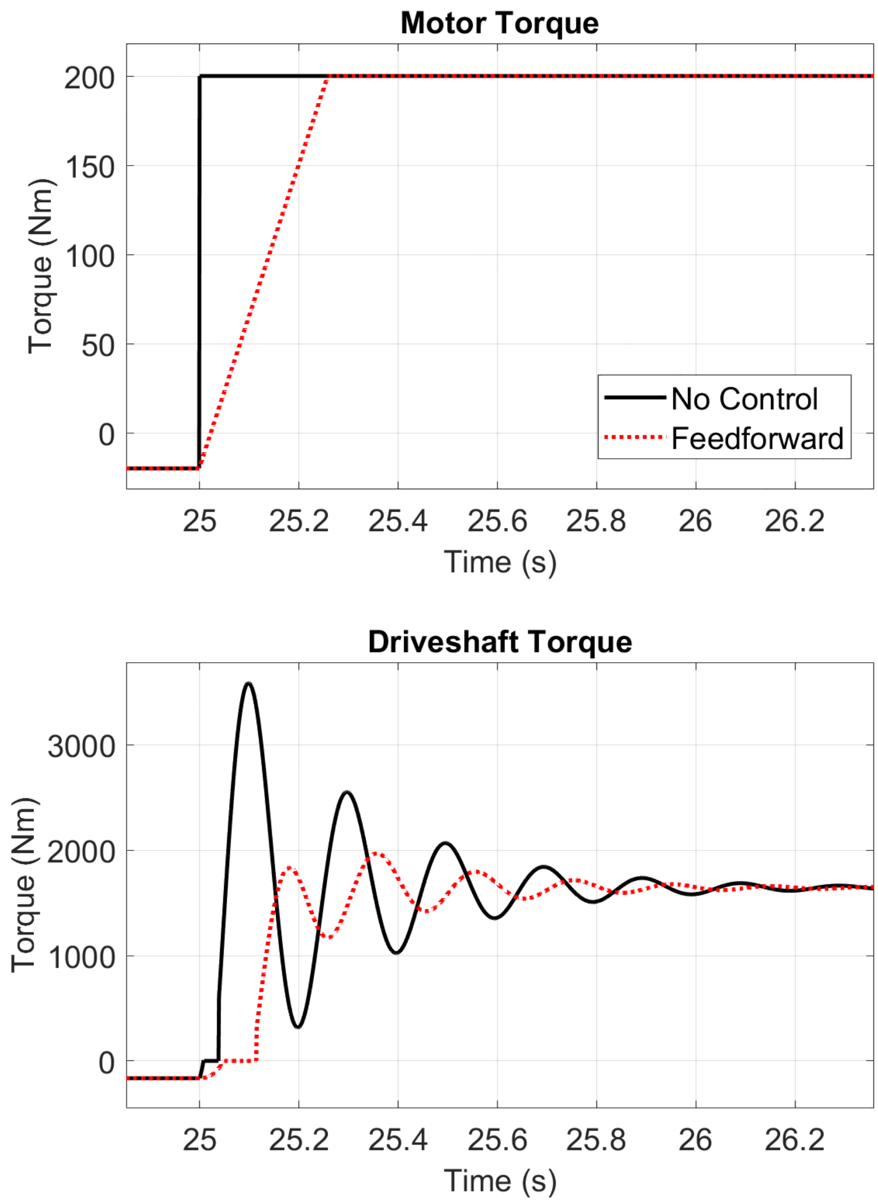

Figure 13a: Feedforward vs. open-loop tip-in maneuver with backlash traversal

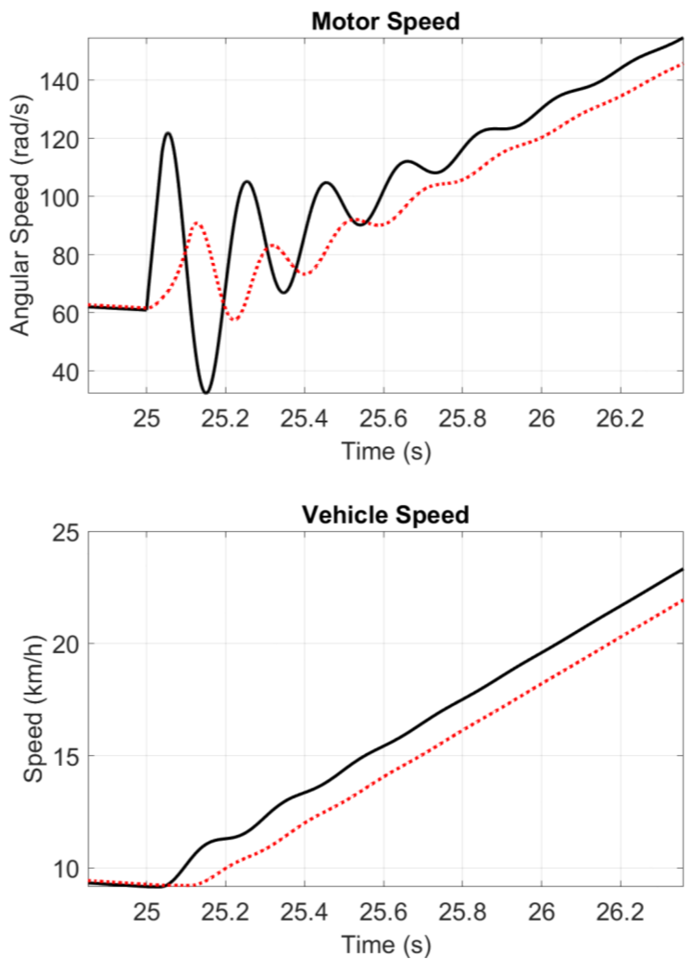

Figure 13b: Feedforward vs. open-loop tip-in maneuver with backlash traversal

To reduce the remaining vibrations after a tip-in or tip-out event, a feedback controller is implemented in the next chapter.

VI. Feedback Control

To further dampen the remaining oscillations after the feedforward controller, a feedback controller based on explicit model predictive control is implemented. The presence of backlash in the model significantly complicates the feedback control design since it makes the system highly nonlinear, and the backlash position cannot be observed especially with how fast backlash traversal can be [8]. Therefore, the robustness of a controller that utilizes a model without the backlash angle state is considered.

Modified Drivetrain Model

The equations of motion derived in second chapter include the backlash angle for both the motor and wheel dynamics. While the backlash position is constant in both negative and positive contact mode, an estimation scheme that can determine which contact mode the system is in based on signals readily available in the vehicle's ECU, such as the motor and wheel speed, was not able to be fully developed for this work. Therefore, the drivetrain dynamics of a model without backlash is used for control design. The physics-based model is given by

$$\dot{\theta}_d(t) = \frac{\omega_m(t)}{i} - \omega_w(t) \tag{22}$$

$$J_m\dot{\omega}_m(t) = T_m(t) - \frac{k}{i}\left(\frac{\theta_m(t)}{i} - \theta_w(t)\right) - \frac{b}{i}\left(\frac{\omega_m(t)}{i} - \omega_w(t)\right) \tag{23}$$

$$J_w\dot{\omega}_w(t) = -T_l(t) + k\left(\frac{\theta_m(t)}{i} - \theta_w(t)\right) + b\left(\frac{\omega_m(t)}{i} - \omega_w(t)\right) \tag{24}$$

where $t \in \Re$ is the continuous time. The model variables are described in Table 2. A major difference of the system without backlash is that the displacement angle θ_d is equivalent to the shaft twist.

The reduced model of Eqs. (22) - (24) is given by

$$\dot{x}(t) = A_c x(t) + B_c(u(t) + d(t)) + B_{cl} l(t) \tag{25}$$

$$y(t) = C_c x(t) \tag{26}$$

where $x(t) = [\theta_d(t),\ \dot{\theta}_d(t)] \in \Re^{2\times1},\ u(t) \in \Re$, and $d(t) \in \Re$ are the state variables, control input, and torque request by the driver, respectively. The sum of $u(t)$ and $d(t)$ indicates the actual motor torque $T_m(t)$, and $l(t)$ represents the load torque $T_l(t)$ which is generally unknown as discussed in Chapter II. The system matrices are given as follows:

$$A_c = \begin{bmatrix} 0 & 1 \\ -k\left(\frac{1}{i^2 J_m} + \frac{1}{J_w}\right) & -b\left(\frac{1}{i^2 J_m} + \frac{1}{J_w}\right) \end{bmatrix} \in \Re^{2\times2} \tag{27}$$

$$B_c = \begin{bmatrix} 0 & \frac{1}{iJ_m} \end{bmatrix}^T \in \Re^{2\times1} \tag{28}$$

$$B_{cl} = \begin{bmatrix} 0 & \frac{1}{J_w} \end{bmatrix}^T \in \Re^{2\times1} \tag{29}$$

$$C_c = [0 \quad 1] \in \Re^{1\times2} \tag{30}$$

The second inertia J_w includes the vehicle mass which makes it much bigger than the first inertia J_m, and the load torque $T_l(t)$ is significantly smaller than the motor torque $T_m(t)$ in the low motor speed range where jerking is prominent. Therefore, the impact of the load torque in Eq. (25) can be neglected.

The discrete time model of Eqs. (25) and (26) is given by

$$x(k+1) = A_d x(k) + B_d(u(k) + d(k)) \tag{31}$$

$$y(k) = C_d x(k) \tag{32}$$

where $A_d = \exp(A_c t_s),\ B_d = A_c^{-1}(A_d - I)B_c$, and $C_d = C_c$. The discrete time is indicated by $k \in \mathbb{Z}$ and the sampling time is indicated by t_s. Going forward, the subscript *d* will be omitted for simplicity.

Anti-Jerk Control Design

The proposed anti-jerk control consists of the rate limiting feedforward controller, reference generator, state observer, and explicit MPC as shown in Fig. 14.

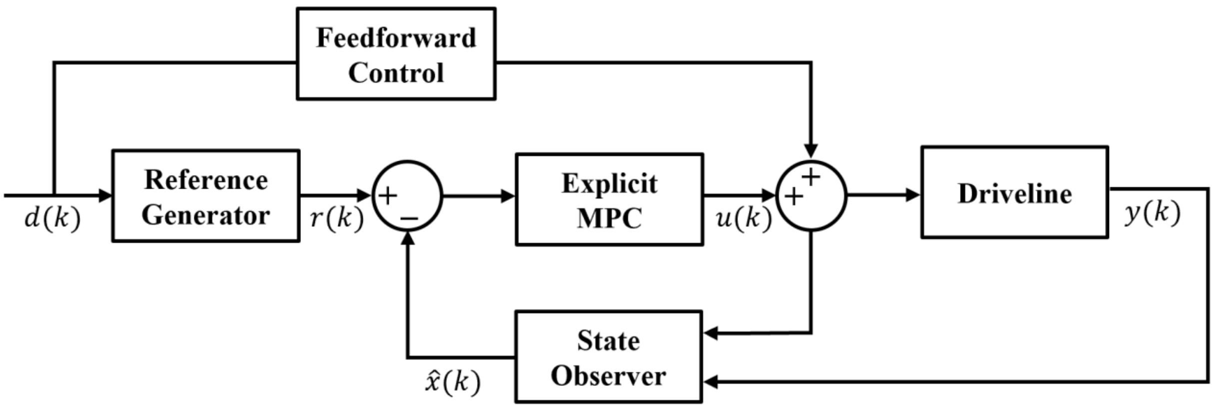

Figure 14: Block diagram of overall anti-jerk control

The reference generator generates the reference variables $r(k) = \left[\theta_{d,ref}(k),\ \dot{\theta}_{d,ref}(k)\right]^T$ to be tracked without dynamic consideration. The state observer estimates the state variables $\hat{x}(k) = \left[\hat{\theta}_d(k),\ \hat{\dot{\theta}}_d(k)\right]^T$ to follow the reference. The eMPC finds the control input $u(k)$ from the proposed optimization problem presented in the next sections.

Explicit Model Predictive Control

The principle of the MPC scheme is shown in Fig. 15. The optimal predicted control input is computed over the finite output prediction horizon length N_p so that the predicted output tracks the reference while satisfying the given constraints. Additionally, only the first control input is implemented into the actual plant, and the optimization process is repeated at each time step.

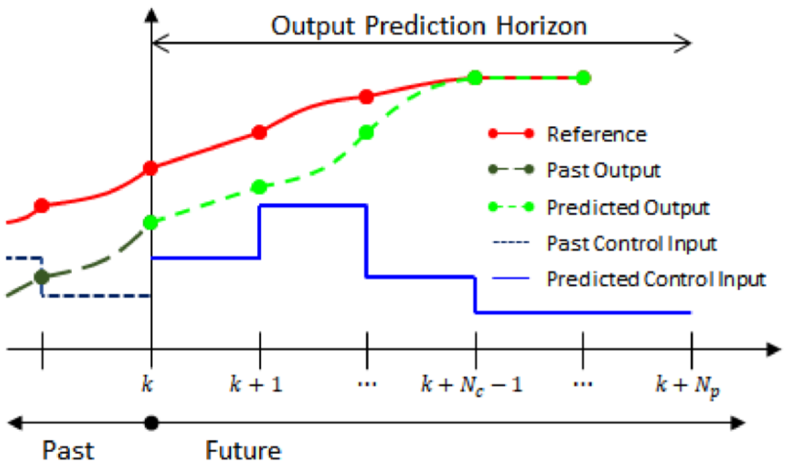

Figure 15: Model predictive control scheme

As can be seen on the horizontal axis in Fig. 15, the control prediction horizon N_c can differ from the output prediction horizon N_p which improves computational efficiency. The predicted control input remains the same after the control prediction horizon such that

$$u(i|k) = u(i-1|k) + \Delta u(i|k) \tag{33}$$

$$\Delta u(i|k) = 0 \quad \forall i \geq N_c \tag{34}$$

where $\Delta u(i|k)$ indicates the *i*-th predicted control input change ahead at time *k*.

In the proposed eMPC scheme, the following LQR-type cost function is employed over the finite production horizon:

$$J(k) = \frac{1}{2}\sum_{i=1}^{N_p}\big(r(i|k) - x(i|k)\big)^T Q\big(r(i|k) - x(i|k)\big) + \frac{1}{2}\sum_{i=0}^{N_c-1} \Delta u(i|k)^T R \Delta u(i|k) \tag{35}$$

where $Q \in \Re^{n\times n}$ and $R \in \Re^{r\times r}$ are the diagonal weighting matrices. The state vector and control input have dimensions *n* and *r*, respectively. The first term of Eq. (35) is to force reference tracking, and the second term is a soft constraint that minimizes the change of the control input. The objective of the proposed eMPC scheme is to find the optimal control input change

$\Delta u(i|k)\ \forall i \in \{0, 1, \dots, N_c - 1\}$ that minimizes Eq. (35). Then, the control input prediction $u(i|k)\ \forall i \in \{0, 1, \dots, N_p - 1\}$ can be calculated from Eqs. (33) and (34).

Using Eq. (31), the state prediction over the N_p prediction horizon length can be obtained with the following:

$$X(k) = Fx(k) + G(u(k-1) + d(k)) + H\Delta U(k) \tag{36}$$

$X(k)$ and $\Delta U(k)$ are the sets of predicted state and control input up to N_p and $N_c - 1$, respectively. They can be expressed as

$$X(k) = \begin{bmatrix} x(1|k) \\ x(2|k) \\ \vdots \\ x(N_c|k) \\ x(N_c+1|k) \\ \vdots \\ x(N_p) \end{bmatrix}, \qquad \Delta U(k) = \begin{bmatrix} \Delta u(0|k) \\ \Delta u(1|k) \\ \vdots \\ \Delta u(N_c - 1|k) \end{bmatrix}$$

The matricies $F \in \Re^{nN_p \times n}$, $G \in \Re^{nN_p \times r}$, and $H \in \Re^{nN_p \times rN_c}$ are given below:

$$F = \begin{bmatrix} A \\ A^2 \\ \vdots \\ A^{N_c} \\ A^{N_c+1} \\ \vdots \\ A^{N_p} \end{bmatrix}, \qquad G = \begin{bmatrix} B \\ (A + I_n)B \\ \vdots \\ (A^{N_c-1} + \cdots + I_n)B \\ (A^{N_c} + \cdots + I_n)B \\ \vdots \\ (A^{N_p-1} + \cdots + I_n)B \end{bmatrix}$$

$$H = \begin{bmatrix} B & 0 & \dots & 0 \\ (A + I_n)B & B & 0 & 0 \\ \vdots & & \ddots & 0 \\ (A^{N_c-1} + \cdots + I_n)B & \cdots & \cdots & B \\ (A^{N_c} + \cdots + I_n)B & \cdots & \cdots & (A + I_n)B \\ \vdots & & & \vdots \\ (A^{N_p-1} + \cdots + I_n)B & \dots & \dots & (A^{N_p-N_c} + \cdots + I_n)B \end{bmatrix}$$

where I_n is the *n*-by-*n* identity matrix.

The future torque request by the driver is not known, so the reference generator assumes the identical reference over the prediction horizon length such that

$$X_r(k) = \begin{bmatrix} r(1|k) \\ \vdots \\ r(N_p|k) \end{bmatrix} = \begin{bmatrix} r(k) \\ \vdots \\ r(k) \end{bmatrix} = F_r d(k) \tag{37}$$

where $F_r = [I_n,\ I_n \ldots\ I_n]^T (I_n - A)^{-1} B$

Then, by using Eqs. (36) and (37), the cost function of Eq. (35) can be rewritten by Eq. (38) and further by Eq. (39).

$$J(k) = \frac{1}{2}(X_r(k) - X(k))^T \bar{Q}(X_r(k) - X(k)) + \frac{1}{2}\Delta U(k)^T \bar{R} U(k) \tag{38}$$

$$J(k) = \frac{1}{2}\Big(F_r d(k) - Fx(k) - G\big(u(k-1) + d(k)\big) - H\Delta U(k)\Big)^T \bar{Q}\Big(F_r d(k) - Fx(k) - G\big(u(k-1) + d(k)\big) - H\Delta U(k)\Big) + \frac{1}{2}\Delta U(k)^T \bar{R} U(k) \tag{39}$$

where $\bar{Q} = blockdiag(Q, \ldots, Q) \in \Re^{(nN_p)\times(nN_p)}$ and $\bar{R} = blockdiag(R, \ldots, R) \in \Re^{(rN_c)\times(rN_c)}$.

The optimality condition $\frac{\partial J(k)}{\partial \Delta U(k)} = 0$ yields the optimal control input change given by

$$\Delta U(k) = (H^T \bar{Q} H + \bar{R})^{-1} H^T \bar{Q}\big((F_r - G)d(k) - Fx(k) - Gu(k-1)\big) \tag{40}$$

Moreover, the first component to be implemented into the actual plant is obtained by

$$\Delta u(k) = \Delta u(0|k) = O\Delta U(k) \tag{41}$$

where $O = [I_r, 0, \ldots, 0] \in \Re^{r\times(rN_c)}$.

From Eqs. (33), (40), and (41), the optimal control input from the proposed eMPC can be written by

$$u(k) = \alpha d(k) + \beta x(k) + (1 + \gamma)u(k-1) \tag{42}$$

where α, β, and γ are given by

$$\alpha = O(H^T \bar{Q} H + \bar{R})^{-1} H^T \bar{Q}(F_r - G)$$

$$\beta = -O(H^T \bar{Q} H + \bar{R})^{-1} H^T \bar{Q} F$$

$$\gamma = -O(H^T \bar{Q} H + \bar{R})^{-1} H^T \bar{Q} G$$

State Feedback Control

The state feedback control with the gain matrix $K \in \Re^{r \times n}$ is given by

$$u_{fb}(k) = Ke(k) = K(r(k) - x(k)) = K((I_n - A)^{-1}Bd(k) - x(k)) \tag{43}$$

Eqs. (33) and (34) include terms with the functions $d(k)$ and $x(k)$. These coefficients of these terms can be equated together, i.e. $\alpha = K(I_n - A)^{-1}$ and $\beta = -K$, and the gain matrix K can be obtained. The eMPC solution of Eq. (42) can then be rewritten by the state feedback control and low pass filter as given by

$$u(k) = \frac{Ke(k)}{1-(1+\gamma)q^{-1}} \tag{44}$$

where q^{-1} is a unit delay operator. Eq. (44) is beneficial since its implementation is much easier than Eq. (42).

The coefficients α, β, and γ are functions of model parameters which means that the optimal gain matrix K and filter constant γ are as well. A model parameter such as vehicle mass can vary due to factors such as the number of passengers. Many electric vehicles in production are equipped with a single gear ratio, but some electric vehicles can have multiple gear ratios. Whether it is a different vehicle mass or number of gear ratios, control parameters can be computed offline and mapped to a specific set of vehicle parameters [24].

State Observer

In order for the proposed eMPC to solve the state tracking problem, the state variables need to be estimated from the driven measurements. The torsion rate, which is the output given in Eq. (32), can be obtained from Eq. (22) using the readily available signals of motor and wheel speed from the vehicle ECU. For state estimation, the following Luenberger state observer is used:

$$\hat{x}(k+1) = A_d\hat{x}(k) + B_d(u(k) + d(k)) + L(y(k) - C_d\hat{x}(k)) \tag{45}$$

The observer gain $L \in \Re^{2\times1}$ is designed using pole placement so that the eigenvalues of $(A_d - LC_d)$ lie within the unit circle of the complex plane.

The observer behavior for a system without damping control is shown in Fig. 16 with a tip-in request without backlash traversal at a time of 2 seconds and a tip-out request with backlash traversal at a time of 4 seconds. For the first tip-in request, the observer is able to estimate the oscillations in the torsion angle and torsion rate well since contact mode is retained throughout the event. When a tip-out event occurs and the backlash gap opens several times, the system becomes unobservable as evident by the deviations in the torsion angle and torsion rate. After the system maintains negative contact mode at a time of 4.65 seconds, the observer can converge and accurately estimate the torsion angle and rate.

Simulation Results

The eMPC-based anti-jerk control is validated using numerical simulations. The vehicle parameters used are displayed in Table 2. Figures 17 to 19 show simulations results with feedforward (FF) only control, FF with the proposed eMPC ($N_p = 30$ and $N_c = 10$), and FF with an LQR controller to be used as a benchmark. The same weighting matricies, Q and R, are used for both the eMPC and LQR controller.

It can be seen from Figures 17 to 19 that both LQR and eMPC dampen torsional vibrations at least within the first two periods compared to a system with only feedforward control. The eMPC even does so in one less period than the LQR. The tradeoff between damping and responsiveness is evident in these simulations. The proposed eMPC features better damping, whereas the LQR control features less loss in performance and responsiveness. However, the better damping of the eMPC is especially favorable during the tip-out event. In Fig. 18, the eMPC causes the system to enter backlash mode only once while the LQR enters backlash mode twice as shown with the zeroing of the torsion angle and rate. By preventing the system from opening the backlash gap more than once, the eMPC reduces the amount of clunk heard and improves the longevity of parts in the driveline.

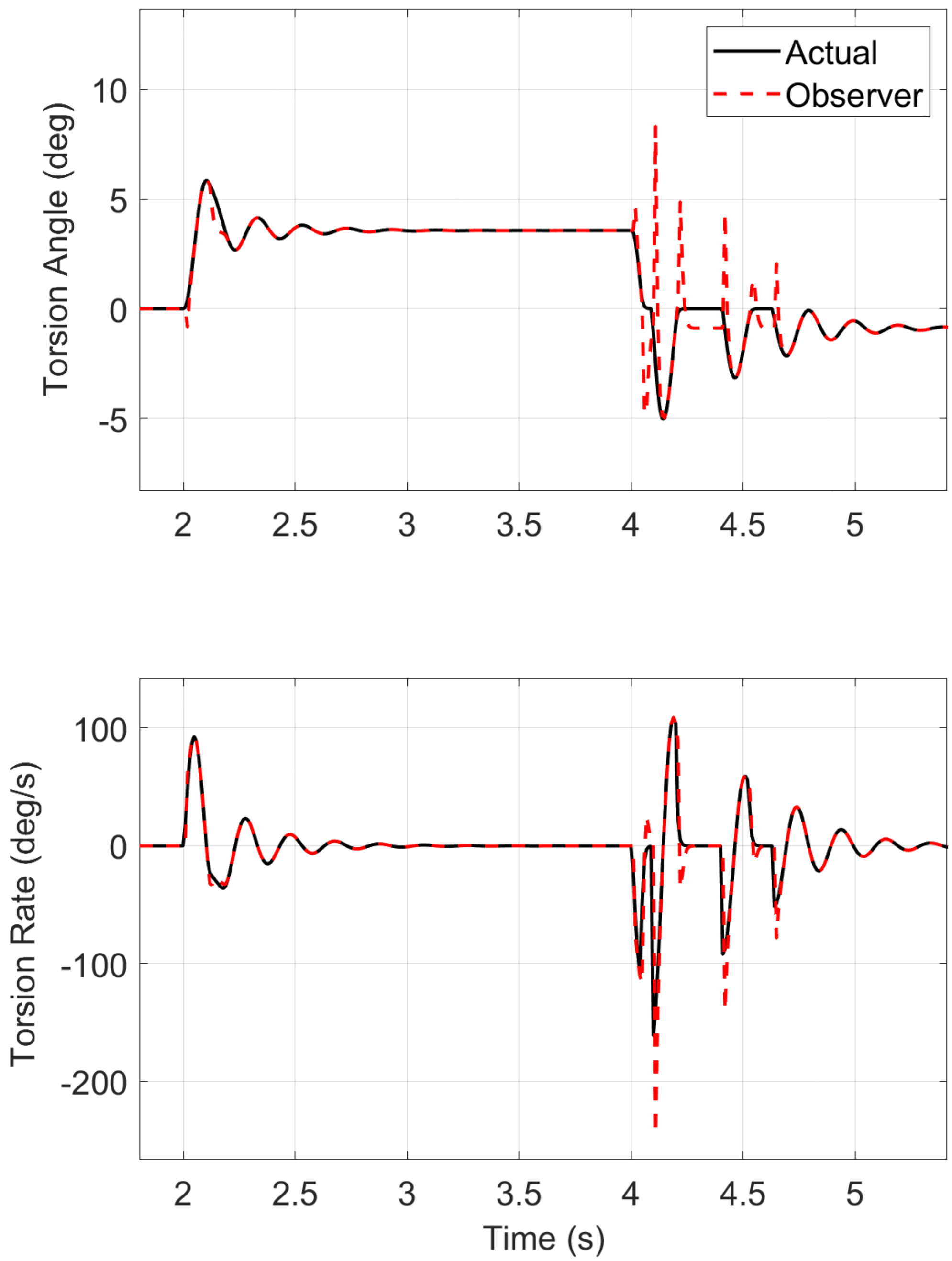

Figure 16: Observer behavior for a system without damping control during a tip-in event without backlash traversal and a tip-out event with backlash traversal

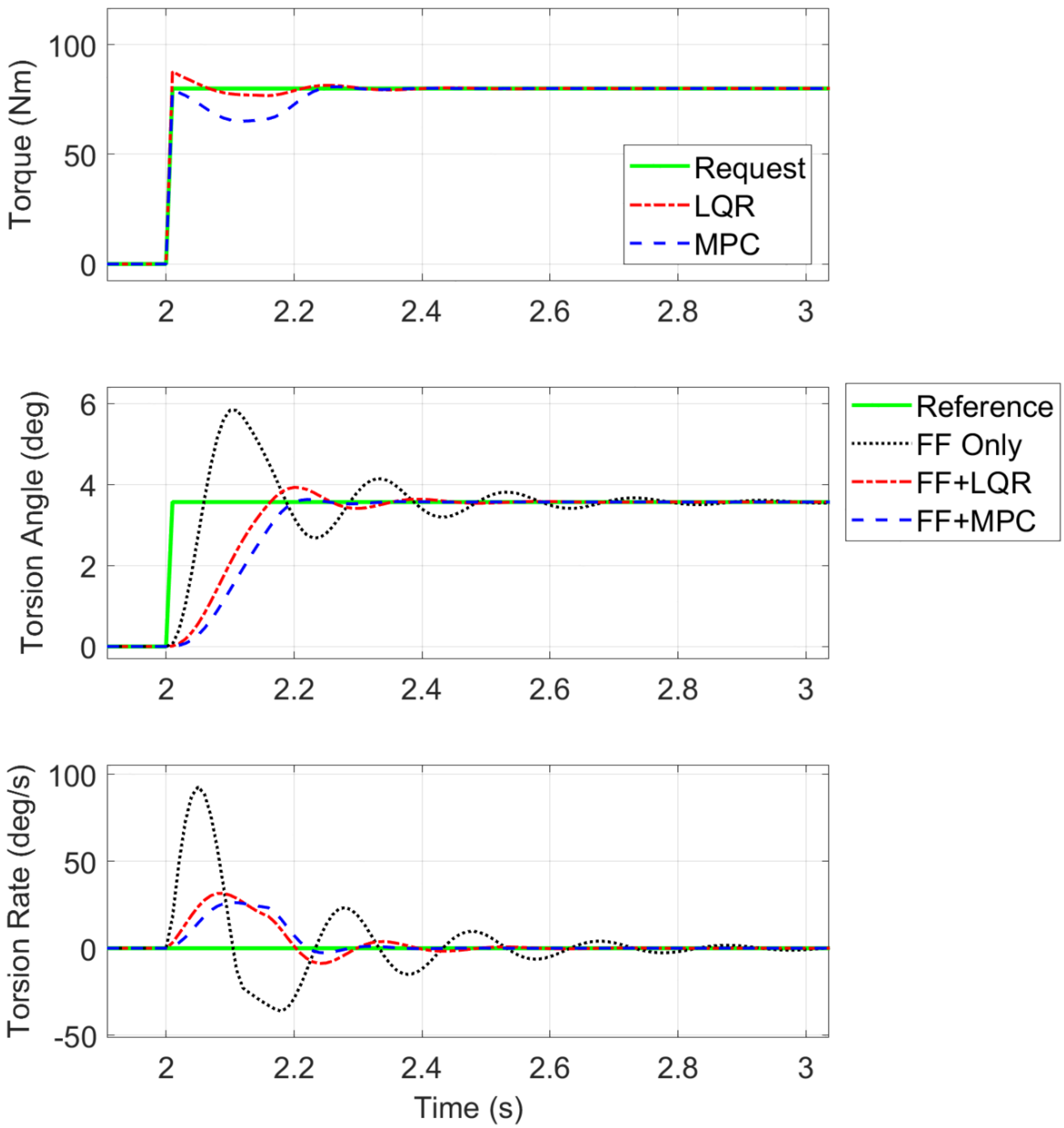

Figure 17: Feedforward and feedback control vs feedforward only control of a tip-in maneuver with no backlash traversal

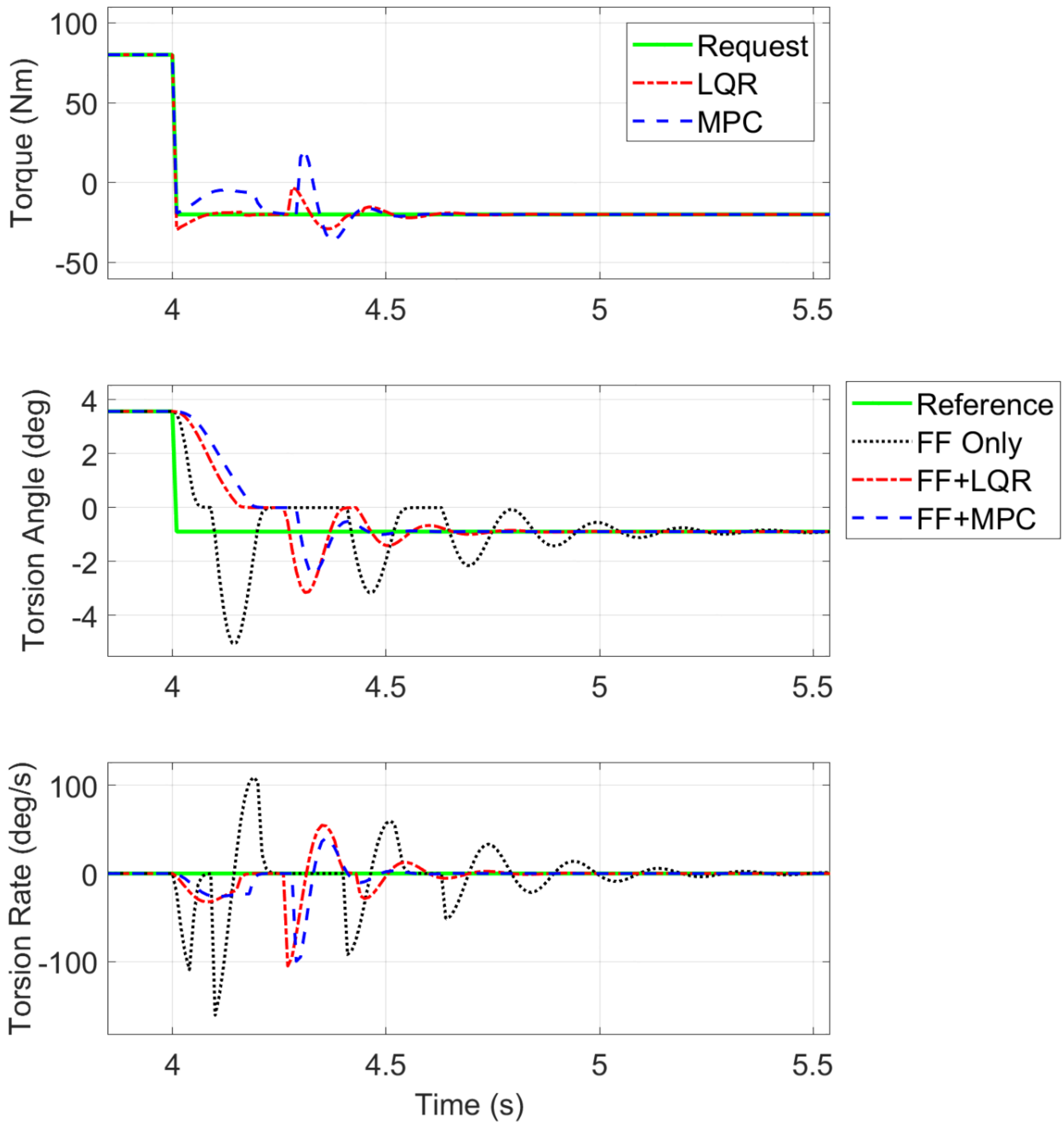

Figure 18: Feedforward and feedback control vs feedforward only control of a tip-out maneuver with backlash traversal

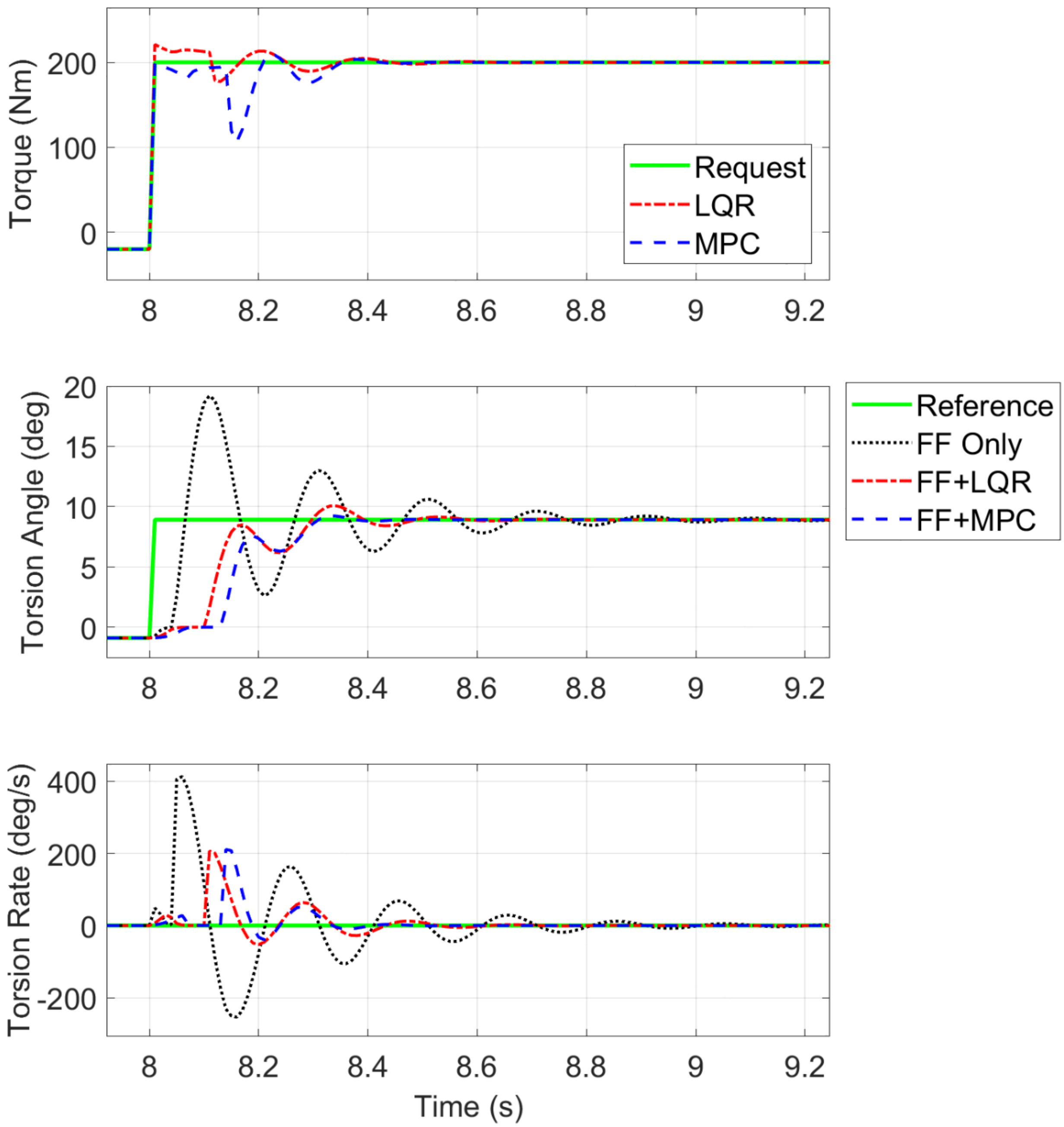

Figure 19: Feedforward and feedback control vs feedforward only control of a tip-in maneuver with backlash traversal

VII. Conclusion

Electric vehicles lack the same damping elements that are present in traditional internal combustion engine vehicles such as a torque converter or clutches. Therefore, electric vehicles are more susceptible to unpleasant vibrations in the low frequency band which causes discomfort to vehicle occupants and reduces the lifespan of drivetrain components. In this work, the mathematical model of an electrified drivetrain with backlash was derived and programmed in Simulink, and torque profiling is paired with explicit model predictive control to dampen torsional vibrations in the drivetrain and reduce vehicle jerk. For the eMPC scheme, the optimal solution is calculated offline and implemented as the state feedback control and low pass filter which is computationally cheap, making it feasible to implement in a real vehicle. Control parameters are saved as a map of vehicle parameters with the assumption they are available from a separate control unit. While the eMPC was formulated using a linear model that neglected backlash, it was robust enough to dampen torsional vibrations without significant loss to responsiveness in a system with backlash.

VIII. Future Work

To further reduce jerking, the possibility of using machine learning to formulate an optimal feedforward controller will be investigated. Addressing the observer and controller performance during backlash traversals, a controller that is able to switch modes depending on the mode of the drivetrain will also be investigated.

IX. Biographical Note

Jomar-Christian Noceda will be receiving a Bachelor of Science in Mechanical Engineering from the School of Engineering and Computer Science, Oakland University, in December 2022. He is very grateful for his mentor, Dr. Yongsoon Yoon, who expanded his interest in controls and provided considerable guidance on theory and research. Jomar plans to work for an automotive manufacturer and strives to be a control engineer in the automotive industry. He also wishes to pursue a Master of Science in Mechatronic Systems Engineering at Oakland University to further his knowledge of control systems and theory. While pursuing his master's degree, he would like to perform controls research involving electric vehicles which are a considerable passion to him and are becoming increasingly adopted in the automotive industry.

References

[1] M. Ehsani, Y. Gao, S. Longo and K. Ebrahimi, *Modern Electric, Hybrid Electric, and Fuel Cell Vehicles*. Boca Raton, FL, USA: Taylor & Francis Group, 2018.

[2] "Inventory of U.S. Greenhouse Gas Emissions and Sinks: 1990-2019," U.S. Environmental Protection Agency, Apr. 2021. [Online]. Available https://www.epa.gov/sites/default/files/2021-04/documents/us-ghg-inventory-1990-2019-data-highlights.pdf

[3] "Sources of Greenhouse Gas Emissions", U.S. Environmental Protection Agency, Aug. 2022. [Online]. Available https://www.epa.gov/ghgemissions/sources-greenhouse-gas-emissions

[4] K. Ronayne, "California moves toward phasing out sale of gas-powered vehicles by 2035," *PBS*, Aug. 25, 2022. [Online]. Available: https://www.pbs.org/newshour/nation/california-moves-toward-phasing-out-sale-of-gas-powered-vehicles-by-2035

[5] "Global EV Outlook 2022," IEA, May 2022. [Online]. Available: https://www.iea.org/reports/global-ev-outlook-2022

[6] M. Batra, "Dynamics and Model-Predictive Anti-Jerk Control of Connected Electric Vehicles," Ph.D. dissertation, University of Waterloo, Waterloo, ON, CA, 2018.

[7] R. Guo, H. Chen and M. Wang, "Modeling and active control of power-split hybrid electric vehicle launch vibration," *Journal of Low Frequency Noise, Vibration and Active Control*, vol. 38, no. 2, pp. 592-607, 2018.

[8] A. Lagerberg and B. Egardt, "Evaluation of Control Strategies for Automotive Powertrains with Backlash," *AVEC 2002*, Hiroshima, JP, September 9-13, 2002.

[9] P. Reddy, K. Darokar, D. Robinette, M. Shahbakhti and J. Blough, “Control-Oriented Modeling of a Vehicle Drivetrain for Shuffle and Clunk Mitigation,” SAE Technical Paper 2019-01-0345, Apr. 2019, doi:10.4271/2019-01-0345

[10] J. Sainio, “Backlash compensation in electric vehicle powertrain,” M.S. thesis, Dept. Elect. Eng., Aalto Univ., Espoo, Finland, 2016.

[11] M. Nordin and P. Gutman, “Controlling mechanical systems with backlash−a survey,” *Automatica*, vol. 38, no. 10, pp. 1633-1649, 2002.

[12] P. Reddy, M. Shahbakhti, M. Ravichandran and J. Doering, “Drivetrain clunk control via a reference governor,” *IFAC Papers Online*, vol. 54, no. 20, pp. 846-851, 2021.

[13] P. Templin and B. Egardt, “A Powertrain LQR-Torque Compensator with Backlash Handling,” *Oil & Gas Science and Technology*, vol. 66, no. 4, pp. 645-654, 2011.

[14] A. Scamarcio, P. Gruber, S. Pinto and A. Sorniotti, “Anti-jerk controllers for automotive applications: A review,” *Annual Reviews in Control*, vol. 50, pp. 174-189, 2020.

[15] W. Wang, Y. Li, J. Shi and C. Lin, "Vibration Control Method for an Electric City Bus Driven by a Dual Motor Coaxial Series Drive System Based on Model Predictive Control," in *IEEE Access*, vol. 6, pp. 41188-41200, 2018, doi: 10.1109/ACCESS.2018.2859356.

[16] C. Rostiti et al., “A Backlash Compensator for Drivability Improvement Via Real-Time Model Predictive Control,” Journal of Dynamic Systems, Measurement, and Control, vol. 140, pp. 104501-(1-10), 2018.

[17] M. Batra, A. Maitland, J. McPhee and N. L. Azad, "Non-Linear Model Predictive Anti-Jerk Cruise Control for Electric Vehicles with Slip-Based Constraints," 2018 Annual American Control Conference (ACC), 2018, pp. 3915-3920, doi: 10.23919/ACC.2018.8431389.

[18] M. Nordin, J. Galic and P. Gutman, “New Models for Backlash and Gearplay,” *International Journal of Adaptive Control and Signal Processing*, vol. 11, pp. 49-63, 1997.

[19] K. Ogata, *System Dynamics*, 4th ed. Upper Saddle River, NJ, USA: Pearson Prentice Hall, 2004.

[20] G. Guercioni, E. Galvagno, A. Tota, A. Vigliani and T. Zhao, "Driveline Backlash and Half-shaft Torque Estimation for Electric Powertrains Control," SAE Technical Paper 2018-01-1345, 2018, https://doi.org/10.4271/2018-01-1345

[21] T. Pham and L. Bushnell, "Two-degree-of-freedom damping control of driveline oscillations caused by pedal tip-in maneuver," *2015 American Control Conference (ACC)*, 2015, pp. 1425-1432, doi: 10.1109/ACC.2015.7170933.

[22] T. Karikomi, K. Itou, T. Okubo and S. Fujimoto, "Development of the Shaking Vibration Control for Electric Vehicles," *2006 SICE-ICASE International Joint Conference*, 2006, pp. 2434-2439, doi: 10.1109/SICE.2006.315138.

[23] Y. S. Kim, J. Park, T. W. Park, J. S. Bang and H. S. Sim, "Anti-jerk controller design with a cooperative control strategy in Hybrid Electric Vehicle," *8th International Conference on Power Electronics - ECCE Asia*, 2011, pp. 1964-1968, doi: 10.1109/ICPE.2011.5944444.

[24] Y. Yoon, Y. An, Y. Park and H. Kim, “Model Predictive Control for Drivability Enhancement with Input Dead-Segment,” *in Proc Int Conf Control*, *Autom, Systems (ICCAS)*, pp. 916-921, Ilsan, Gyeonggi-do, S. Korea, 2010.